Development of the Retrieval Algorithm and Capability Study of Ozone for JEM/SMILES

(JEM/SMILES に対するリトリーバルアルゴリズムの開発とオゾン観測可能性の研究)

Chikako Takahashi
髙橋 千賀子

Contents

List of Tables

List of Figures

Abstract

The Superconducting Submillimeter-Wave Limb-Emission Sounder (SMILES) have been launched and aboard the Japanese Experiment Module (JEM) of the International Space Station (ISS) in September 2009. It had measured the submillimeter wave limb emission from atmospheric minor species mainly in the stratosphere. It is the first to use 4-K mechanical refrigerator to cool superconducting devices and a major feature of the SMILES is very sensitive measurements by low system noise temperature. It achieved approximately 400 K. The SMILES requires the high accuracy and fast for the retrieval algorithm, because the SMILES has very high sensitivity thanks to superconducting receiver and retrieves the density distributions of the target species from calibrated spectra in near-real-time.

The retrieval algorithm is based on the optimal estimation method applied for atmospheric soundings by C. Rodgers. The retrieval process consists of two parts: the forward model, which computes radiative transfer, and the inverse model, which deduces atmospheric states. The forward model must provide the most accurate basis for results because SMILES has very high sensitivity. Therefore the forward model algorithm for an operational system has to be accurate. It should be fast because of limitation of computing resources. Hence, the algorithm is improved (1) by designing accurate instrument functions such as the instrumental field of view (FOV), sideband rejection ratio of sideband separator, and spectral responses of acousto-optic spectrometer (AOS) and (2) by optimizing radiative transfer calculation. The

accuracy of this algorithm has been achieved better than 1%, and the processing time for single-scan spectra and the processing speed has been achieved faster than 1 min with 8 parallel processing using a 3.16-GHz Quad-Core Intel Xeon processor. In Chapter II show the details of these algorithms.

In Chapter III, we estimate the capability of O_3 retrieving from measurements by SMILES. Since SMILES has very high sensitivity, the ozone retrieval is expected to be highly precision. We examine the retrieval precision and the accuracy of O_3 vertical profiles based on the launch-ready retrieval algorithm developed for the SMILES. The best retrieval precision with single scan spectra is 0.2% at an altitude of 30 km with 3 km vertical resolution in the mid-latitude. The retrieval precision is better than 5% in the altitude region from 15 to 70 km in the nighttime and from 15 to 55 km in the daytime. By averaging 10 profiles, the retrieval precision is improved to 1% at 70 km altitude in the nighttime and to 5% in the daytime. It is expected to reveal the diurnal variation of O_3 vertical profiles with high precision in the upper stratosphere. Moreover, the retrieval capability in the lower stratosphere is estimated. By retrieving spectral data using two receiver bands (624.32 GHz - 626.32 GHz and 649.12 GHz - 651.32 GHz), the retrieval precision at 13 km altitude will be expected to be approximately 3% under clear sky conditions, which is 10 times better than one retrieved from a single band. We have clarified the retrieval capabilities for the diurnal variation in the upper stratosphere, the effects from the model parameters such as the a priori profiles, uncertainty of the atmospheric temperature and the cirrus clouds, and the effectiveness for the simultaneous retrieval of the

lower and upper sidebands in the lower stratosphere. Finally, ozone retrieval with measured data are shown in appendix.

Part I
Introduction

1 Status for Atmospheric Ozone

Ozone is one of the key constituents of the Earth's atmosphere. Most ozone resides in the lower stratosphere in what is commonly known as the ozone layer and extends up to about 50 km altitude (see Figure 1). The remaining ozone, about 10%, is found in the troposphere. The ozone layer plays a major role in shielding us from solar ultraviolet (UV) rays, radiation budget and atmospheric chemistry. Increases in ozone occur near the surface as a result of pollution from human activities (WMO, 2010), recentry.

Stratospheric ozone is naturally formed in chemical reactions involving UV rays and oxygen molecules. The processes of ozone production and destruction are as follow:

$$O_2 + h\nu \rightarrow 2O \tag{1}$$

$$O_2 + O + M \rightarrow O_3 + M. \tag{2}$$

Here, M is a catalytic molecule, such as a nitrogen molecule an oxygen molecule. UV rays ($h\nu$) breaks apart one oxygen molecule (O_2) to produce two oxygen atoms (2 O) and each atom combines with an oxygen molecule to produce an ozone molecule (O_3). The production and destruction of stratospheric ozone is balanced in these reactions. This is not cause of ozone depletion. Reactions of the cause of ozone depletion are refered to the next. Stratospheric ozone is destroyed by reactions involving reactive halogen gases,

which are produced in the chemical conversion of halogen source gases. The processes of ozone destruction are as follow:

$$X + O_3 \rightarrow XO + O_2 \tag{3}$$

$$XO + O \rightarrow X + O_2 \tag{4}$$

$$\Longrightarrow O + O_3 \rightarrow 2O_2. \tag{5}$$

Here, X is a reactive halogen gas, such as chlorine (Cl) or bromine atoms (Br). Global ozone has decreased because the amounts of reactive gases containing chlorine and bromine have increased in the stratosphere.

Since the discovery of the Antarctic ozone hole in the mid 1980s, numerous observations have been performes and understanding for the mechanisms of ozone depletion have been advanced. According to the Ozone Depletion 2010 (WMO, 2010), in the early 1990s the depletion of global total ozone reached a maximum of about 5% below the 1964–1980 average. The depletion has lessened since then and now averages about 3.5% for 2006–2009. The total global accumulation of ozone-depleting substances has slowed and begun to decrease. The Ozone Depletion 2010 (WMO, 2010) refers a prediction that the ozone will be recovered by 2050, but there is still some variability in each climate model.

Meanwhile, a relationship between ozone depletion and climate change is also becoming important issue recentry. The ozone depletion itself is not the principal cause of climate change, but changes in ozone and climate are directly linked. Ozone and the ozone-depleting substances are greenhouse

gases along with carbon dioxide (CO_2). Both of stratospheric and tropospheric ozone absorb infrared radiation but these ozone affect the Earth's surface oppositely. Stratospheric ozone depletion causes a negative radiative forcing (i.e. it leads to a cooling of Earth's surface) and in contrast increases in tropospheric ozone cause a positive radiative forcing (i.e. it leads to a warming of Earth's surface). The mechanisms of the link of the ozone changes and climate changes remain to be clarified, because various factors are mixed complexly. The incleasing the green gases warm the tropospheric temperature but it cool the statrospheric and above temperature. The cooling of the lower strasphere cause the polar stratospheric cloud and it lead to the ozone depletion but the cooling of the upper tropoephere provide incleasing ozone contrastly. Furthermore transport processes of atmosphere are affected by climate changes and changes of transport processes also affect the ozone layer.

Finally, issues of the upper troposphere and lower stratosphere (UT/LS) are mentioned here. UT/LS has an important role in the dynamical processes. In UT/LS, the time scale of ozone change on the dynamical processes is as comparable as that of the photochemical time scale. According to (Holton et al., 1995), the planetary wave induced torque mainly drives the upward motion at equatorial latitudes and the downward motion at mid and high latitudes in the lower stratosphere. At equatorial latitudes, a modulation of the meridional circulation affects the tropopause height and temperature, etc., and all these factors are closely connected with each other. However our knowledge is still insufficiency and comprehensive understand-

ing of these mechanism is needed.

The understanding for the mechanisms of ozone depletion have been advanced but there are still unsolved issues, such as the link with the climate change mentioned above. Figure 3 shows 1980 baseline-adjusted multi-model trend estimates of annually averaged total column ozone and Cly at 50 hPa for the tropics (25°S–25°N, upper row) and midlatitudes (middle row: 35°N–60°N, lower row: 35°S–60°S) with 95% confidence and 95% prediction intervals appearing as light- and dark-gray shaded regions, respectively, about the trend (note the different vertical scale among the panels) (WMO, 2010). There are large difference in these models. Therefore, there are further needs of systematic understandings of ozone chemistry and transport processes. Since there have been various measurements, every ozone-depleting substances have not been measured thoroughly. Measurements for some minor morecules like BrO are stil insufficient. To accelerate the understanding of these issues, accurate and global measurements of three-dimensional and simultaneous measurements of ozone and the ozone-depleting substancess are required. The accurate measurement can reveal not only averaged abundance of minor morecules but it can reveal time variation for abundance of measured morecules finer than the previous measurements. For the accurate measurement, developments of both sensor techniques and data processing algorithms are indispensable. The sensor techniques and the data processing algorithms are refered later.

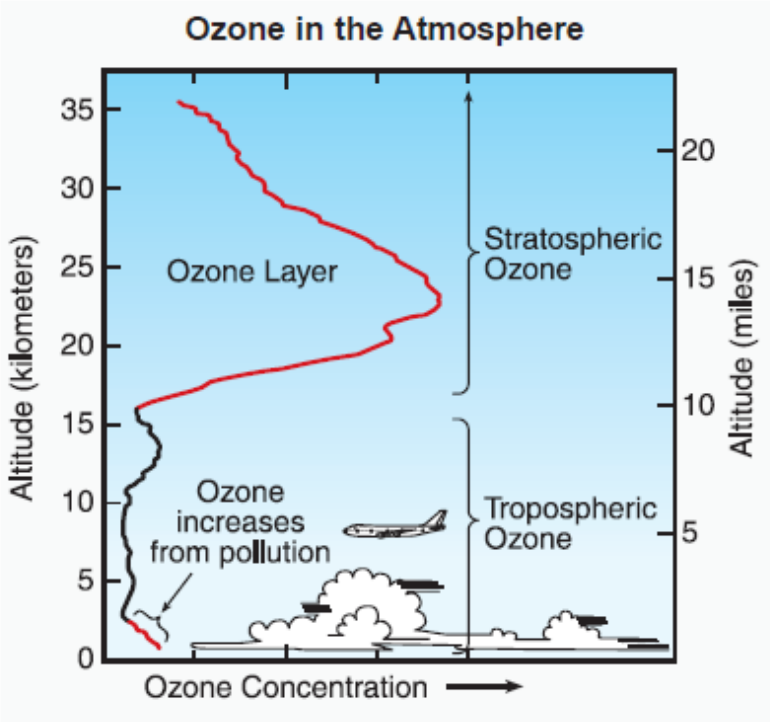

Figure 1: Atmospher ozone destribution by Scientific Assessment of Ozone Depletion 2010 (WMO, 2010)

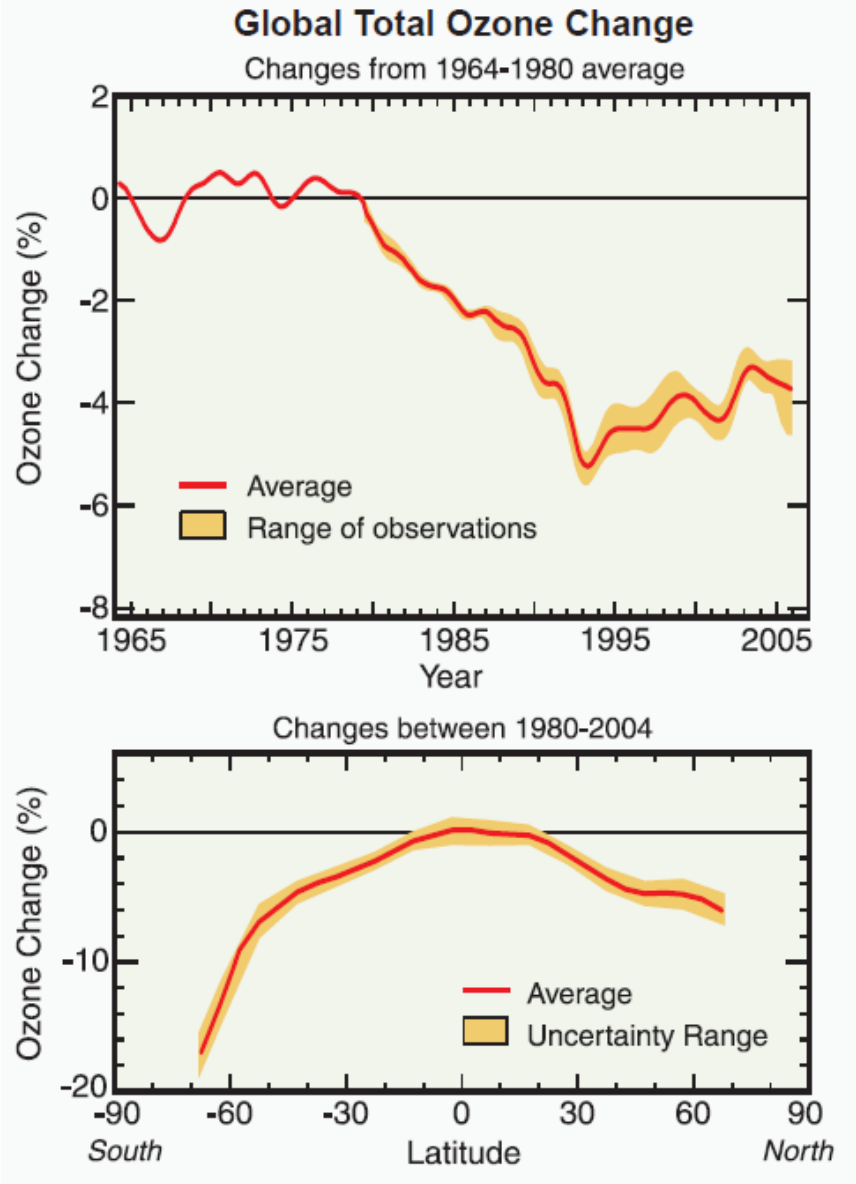

Figure 2: Global total ozone changes by Scientific Assessment of Ozone Depletion 2010 (WMO, 2010)

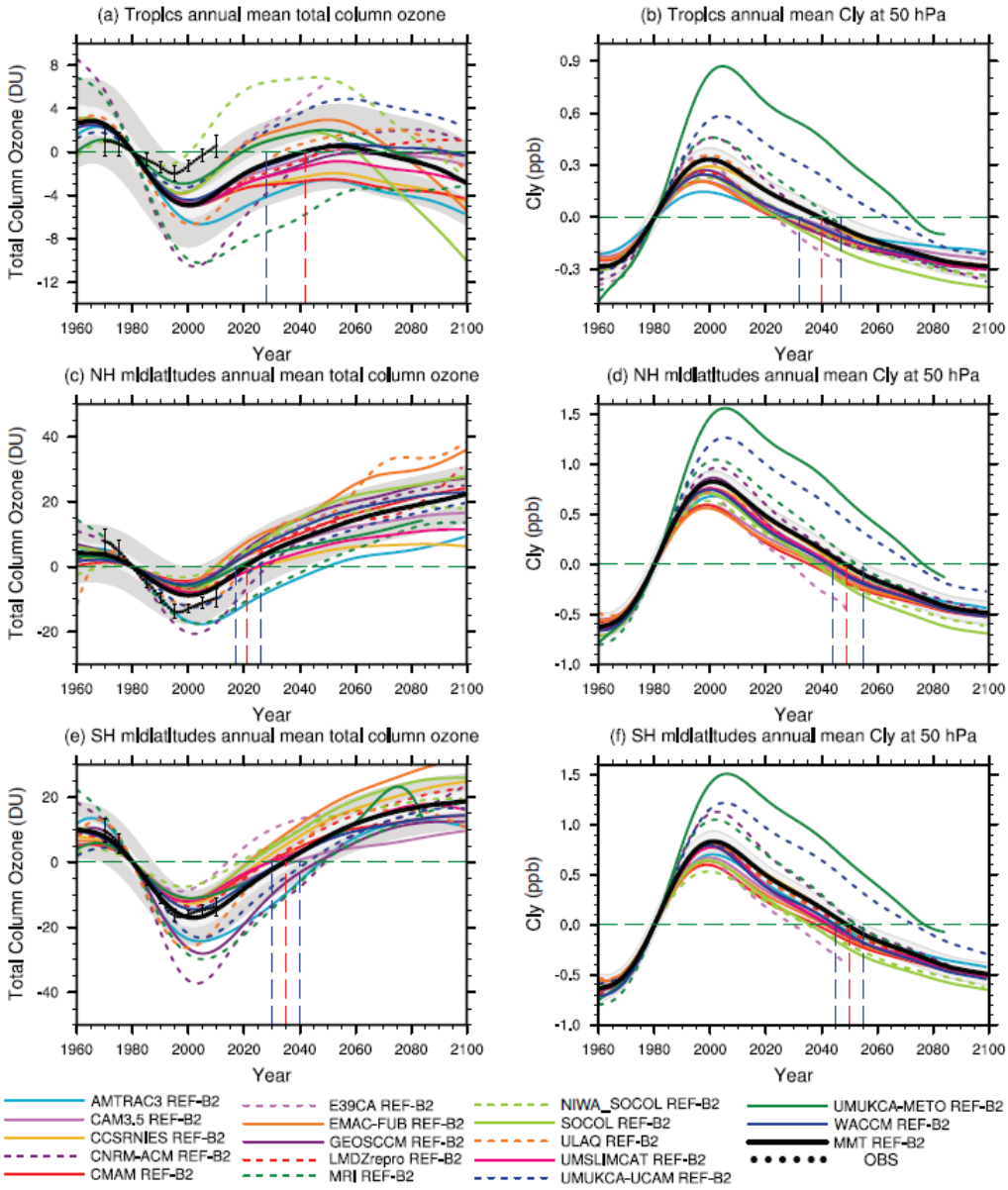

Figure 3: 1980 baseline-adjusted multi-model trend estimates of annually averaged total column ozone (DU; left) and Cly at 50 hPa (ppb; right) for the tropics (25°S–25°N, upper row) and midlatitudes (middle row: 35°N–60°N, lower row: 35°S–60°S) (thick dark gray line) with 95% confidence and 95% prediction intervals appearing as light- and dark-gray shaded regions, respectively, about the trend (note the different vertical scale among the panels) (WMO, 2010).

2 Atmospheric Measurements Techniques

Since the Antarctic ozone hole have been discoverd in the mid 1980s, numerous observations have been conducted and these have helped to revel the mechanism of ozone depletion. Atmospheric ozone have been measured from various platforms, such as the ground, balloons, aircrafts, and satellites.

Total column ozone have been measured from the ground with Dobson spectrophotometers since 1920's. The Dobson spectrometer measures the total ozone by measuring the relative intensity of two ultraviolet wavelength range. It is a standard method for these measurement because of its high sensitive measurements, but it is strongly affected by aerosols and pollutants in the atmosphere. The ground measurement with Umkehr method can mesure the ozone vertical distribution, but its vertical resolution is not so fine. An Ozone laser radar is another technique to measure the atmospheric ozone using laser light and it can meaasure the ozone vertical distributions in the upper stratosphere. It can only work in night time. Othter technique to measure the vertical distributions of ozone is millimeter wave radiometer, which can measure it in the mesosphere in noon and night. Fourier transform infrared spectroscopy (FTIR) is also one of the technique to measure the vertical distributions of ozone and it can measuren not only ozone but also other species like HCl and HNO_3 simultaneously. The ground measurement has advantage to know long-term variability at a certain location but it is difficult to encompass the entire globe finely, but the vertical resolutions are not so fine compared with baloons, aircrafts, ozonesonde and satelite.

Satellites are useful platforms for measureing atmospheric ozone globally and for measureing the vertical distribution with fine resolution up to high-altitude. To measure the vertical distribution with fine resolution, baloons, aircrafts and ozonesonde are useful, but these can also not be cover the entire globe and these can not measure the high altitude region (generally below 30 km). There have been global, long-term and high-quality O_3 measurements by a solar occultation technique with the Stratospheric Aerosol and Gas Experiment (SAGE) series from 1979 to 2005 (Rusch et al., 1997), the Halogen Occultation Experiment (HALOE) (Russell et al., 1993) from 1991 to 2005 and the Polar Ozone and Aerosol Measurement (POAM) (Bevilacqua et al., 1995) from 1993 to 2005. Also the SCISAT/ACE (Atmospheric Chemistry Experiment) mission (Bernath et al., 2005), launched in 2003, uses the solar occultation technique. The Michelson Interferometer for Passive Atmospheric Sounding (MIPAS) launched in 2002 (Fischer and Oelhaf, 1996; Fischer et al., 2008), the Earth Observing System (EOS) Microwave Limb Sounder (MLS)(Read et al., 2006; Froidevaux et al., 2008) instrument launched in 2004, and the Submillimeter Radiometer (SMR) onboard the Odin satellite (Murtagh et al., 2002) launched in February 2001 measure the atmospheric limb emission in infrared, millimeter-wave and submillimeter-wave ranges, respectively. Those emission measurements have the advantage of independence of the solar angle. Furthermore, there are various other types of global ozone measurements. The SCanning Imaging Absorption spectroMeter for Atmospheric CHartographY (SCIAMACHY) (Bovensman et al., 1999) launched in 2002 onboard ENVISAT provides nadir, limb and solar/lunar occultation measurements. Global Ozone Monitoring by Occul-

tation of Stars (GOMOS) also onboard ENVISAT performs the stellar occultation measurements, and the OSIRIS instrument onboard the Odin satellite measures the scattered solar radiation in the visible spectral range.

Submillimeter-wave radiometry techniques are powerful tools for the remote measurements of the earth's middle atmosphere. These techniques allow the simultaneous measurements of a variety of important species for studying atmospheric chemistry and dynamics. The Microwave Limb Sounder (MLS) aboard the Upper Atmosphere Research Satellite (UARS) launched in 1991 has demonstrated that the millimeter-wave limb sounding from satellites is suitable technique for measuring atmospheric constituents and temperature on a global scale (Waters et al., 1999). The first submillimeter limb measurement from space was conducted by the Sub-Millimeter Radiometer (SMR) on board the Odin satellite launched in February 2001 Murtagh et al. (2002). The follow-on MLS aboard the Aura satellite launched in July 2004 measures millimeter and submillimeter bands comprehensively (Read et al., 2006). These technologies have contributed to improving our understanding of stratospheric chemistry.

For future missions, measurements with grobal and high sensitivity are desired in order to study the dynamical features of the atmosphere. These studies require advanced submillimeter measurement technologies, including superconductive receivers with high sensitivity.

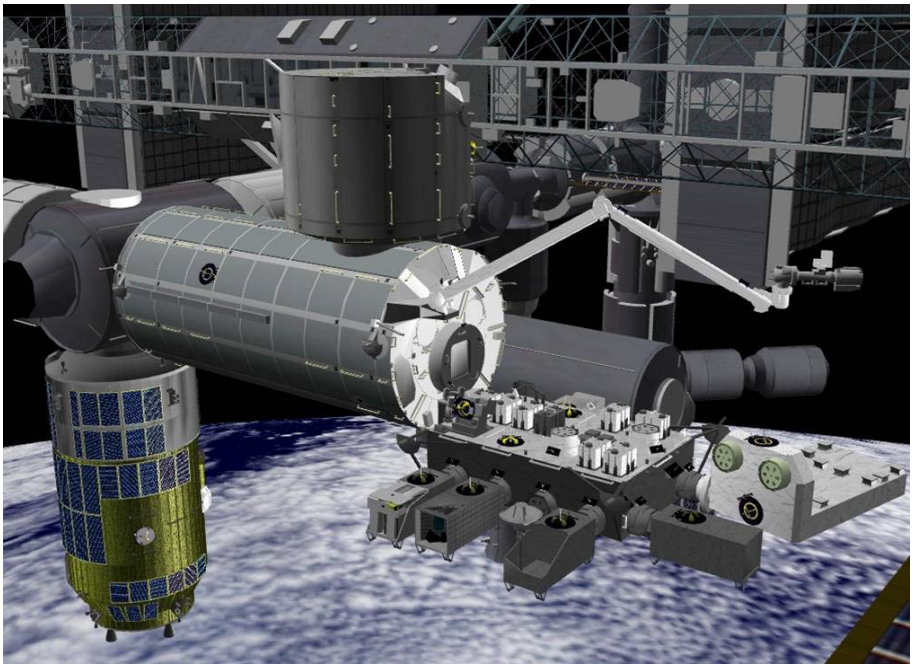

Figure 4: The ISS and SMILES (NASDA and CRL, 2002).

3 JEM/SMILES

The Superconducting Submillimeter-Wave Limb-Emission Sounder (SMILES) instrument has been put in operation as a part of the Japanese Experiment Module (JEM) on board the International Space Station (ISS) since September 2009 (Figure 5). It is a collaborative project between the Japan Aerospace Exploration Agency (JAXA) and the National Institute of Information and Communications Technology (NICT). It measures the submillimeter-wave limb emission from atmospheric minor species mainly in the stratosphere. Figure 6 show the image of the limb observation by SMILES.

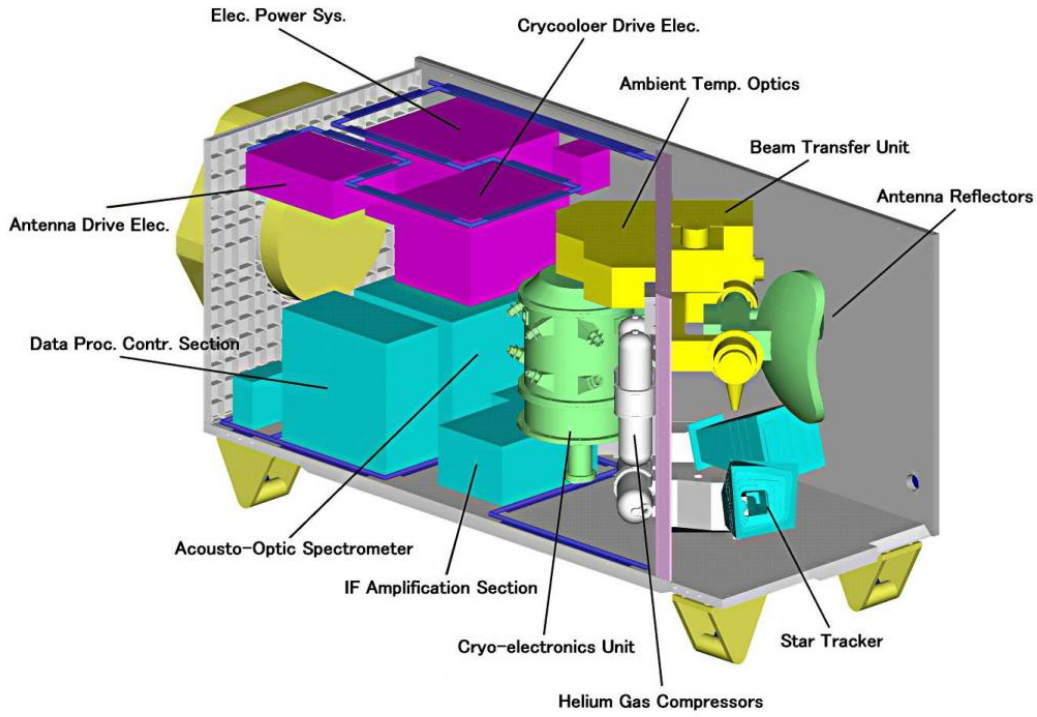

Figure 5: The SMILES payload (NASDA and CRL, 2002).

Table 1: Target species of SMILES

Type	Band A	Band B	Band C
Species retrieved from single-scan data	O_3 $H^{37}Cl$ ^{18}OOO HNO_3 CH_3CN HOCl $O^{17}OO$	O_3 $H^{35}Cl$ ^{18}OOO $O^{17}OO$	O_3 ClO HNO_3 ^{18}OOO ^{17}OOO
Species retrieved from multi-scan data (noisy products)	BrO	HO_2	BrO HO_2

A major feature of JEM/SMILES is the ability to receive high sensitive measurements with a low system-noise temperature using 4–K cooled superconductor-insulator-superconductor (SIS) mixers (Figure **??**. The target species are O_3, ClO, HCl, HNO_3, HOCl, CH_3CN, HO_2, BrO, and O_3 isotopes (See Table1). The SMILES mission focuses on the details of halogen chemistry related to ozone destruction. SMILES takes 53 s for a complete vertical scan and there are 68 individual limb rays in a single scan in the nominal altitude coverage from 10 to 60 km. Since the orbital period of the ISS is approximately 93 min, approximately 105 scans per orbit give 1630 scans per day. The spatial coverage is on a near global basis, or the nominal latitude coverage is 38°S – 65°N by inclining the antenna beam to 45° left from the direction of orbital motion. It is expected that it will be possible to make measurements within the elongated polar vortex in the Northern Hemisphere. The world map of orbit and measurement positions is shown in Figure 7.

Figure 8 shows the block diagram of the SMILES instrument (NASDA

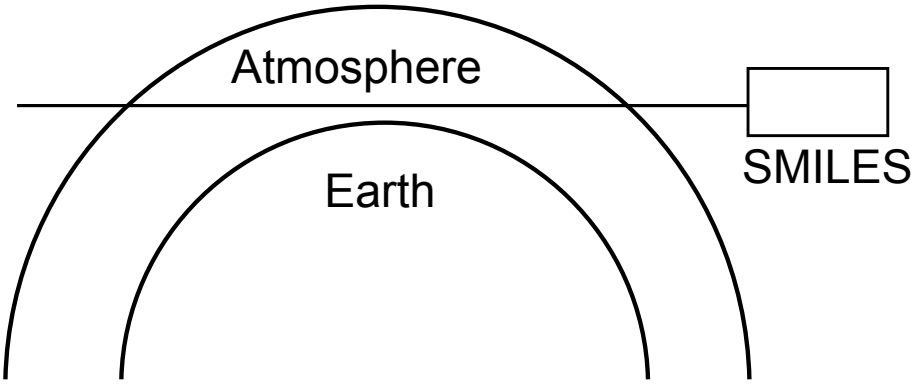

Figure 6: The limb observation by SMILES.

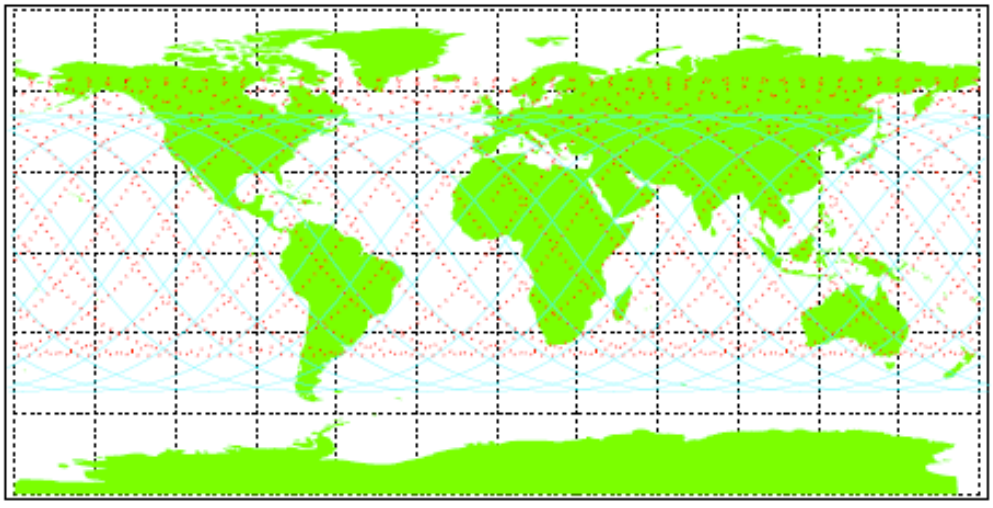

Figure 7: The world map of orbit and measurement positions of SMILES (NASDA and CRL, 2002).

and CRL, 2002). The main components of SMILES are a submillimeter antenna, a submillimeter receiver, and a radio spectrometer. The submillimeter antenna is an elliptical mirror with dimensions of 40 cm invertical direction and 20 cm inhorizontal because of the trade-off between the spatial resolution and the envelope for JEM payloads (Manabe et al., 2008). The vertical beam size is 0.09 degree (half-power beamwidth) and the angular accuracy of the antenna driving mechanism must be better than 0.01 degree. The angular accuracy affects an accuracy of measured altitude determination, which is important factor for retrieval processing. The submillimeter receiver is a key instrument of SMILES experiment and its noise temperature is less than 400 K mentioned above. SMILES has the two SIS mixers that receive the atmospheric signal in the upper sideband (USB) and lower sideband (LSB) separately (USB: 649.12–650.32 GHz, LSB: 624.32–626.32 GHz). The atmospheric emissions are separated by a quasi-optical sideband filter, based on a modiffed Martin-Puplett interferometer (Manabe et al., 2003). A suppression over the other sideband is more than 15 dB but it cannot be ignored in the retrieval processing. The radio spectrometer of SMILES is the acousto-optical spectrometer (AOS) (Ozeki et al., 2000). It analyzes the atmospheric signal and detects its power spectrum. AOS will have two analyzing units with a resolution of 1.8 MHz (full width at half maximum:FWHM) and each power spectrum is obtained with a CCD array of 1728 channels. Table 2 shows the main specifications of SMILES. Further details are given in the SMILES mission plan (NASDA and CRL, 2002) and recent status reports are presented by (Kikuchi et al., 2010) and (Ochiai et al., 2010).

SMILES achieved that the system noise temperature is less than 400 K. In terms of the noise level of the brightness temperature, it is approximately 0.7 K for a single scan. It is better than previous millimeter-submillimeter limb measurements from satellites such as Aura/MLS (Read et al., 2006), whose system noise temperature is approximately 10,000 K at a 600 GHz frequency range, and Odin/SMR (Murtagh et al., 2002), whose system noise temperature is approximately 3,000 K.

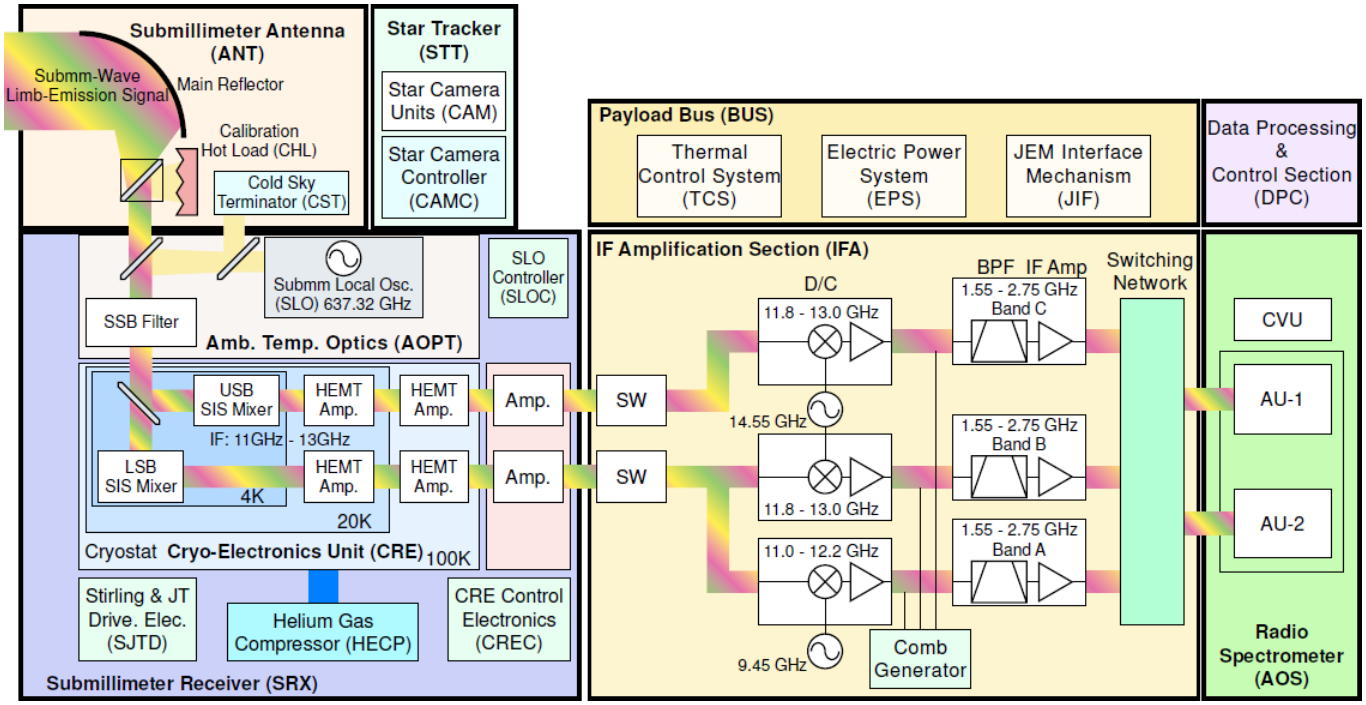

Figure 8: Block diagram of SMILES (NASDA and CRL, 2002).

Table 2: JEM/SMILES Specifications

System Parameter	Description
Frequency bands	Band A (624.3–625.5 GHz)
	Band B (625.1–626.3 GHz)
	Band C (649.1–650.3 GHz)
System noise temperature	Less than 700 K
Instrumental height resolution	3.5–4.1 km (nominal)
Frequency resolution	1.8 MHz (FWHM)
Channel separation	0.8 MHz channel
Integration time	0.5 s for each observation point
Altitude range	10–60 km (nominal)
Global coverage	38°S–65°N (nominal)
Processing time	53 s/scan

4 Retrieval Techniques for JEM/SMILES

The retrieval algorithm for SMILES is based on the standard Optimal Estimation Method (OEM) applied for atmospheric sounding, which is a well-established method used in the field of atmospheric science and has been reported in standard literatures (Rodgers, 1976, 1990, 2000). This section gives a brief outline of the basic retrieval algorithm, and terms and notations used in the subsequent descriptions are defined in Rodgers (2000).

The atmospheric state is represented by a state vector $\mathbf{x}$ of length n. In the SMILES, a state vector represents the vertical profiles of target species concentrations and atmospheric temperature along with other selected parameters described in Chapter II. A measurement vector $\mathbf{y}$ of length m denotes the calibrated brightness temperature observed by the SMILES, and the forward model $\mathbf{F}$ is formulated to describe the brightness temperature according to our knowledge of the physics (including the instrument). A predicted measurement vector $\hat{\mathbf{y}}$ based on the atmospheric state represented by $\mathbf{x}$ and the forward model parameters represented by $\mathbf{b}$ is described by

$$\hat{\mathbf{y}} = \mathbf{F}(\mathbf{x}, \mathbf{b}). \tag{6}$$

The retrieval algorithm is based on the OEM applied for atmospheric sounding (Rodgers, 2000). The most probable solution can be derived from statistical combination of a priori knowledge of $\mathbf{x}$ and the information of the measurement. A priori knowledge is represented by the expected state $\mathbf{x_a}$ and its covariance matrix $\mathbf{S_a}$. The most probable state is the one which

minimizes the χ^2 statistics given by

$$\begin{aligned} \chi^2 &= \{\mathbf{y} - \mathbf{F}(\mathbf{x}, \mathbf{b})\}^{\mathbf{T}} \cdot \mathbf{S_y^{-1}} \cdot \{\mathbf{y} - \mathbf{F}(\mathbf{x}, \mathbf{b})\} \\ &+ (\mathbf{x} - \mathbf{x_a})^{\mathbf{T}} \cdot \mathbf{S_a^{-1}} \cdot (\mathbf{x} - \mathbf{x_a}), \end{aligned} \tag{7}$$

where $\mathbf{S_y}$ is the covariance matrix of $\mathbf{y}$.

The maximum a posteriori estimate can be derived from statistical combination of a priori knowledge of a state vector $\mathbf{x}$ and the information about the measurement. We use a modification of the Gauss-Newton method called the Levenberg-Marquardt method (Levenberg, 1944; Marquardt, 1963). The retrieved state vector $\mathbf{x_{i+1}}$ at the iterative step $i+1$ is calculated as

$$\begin{aligned} \mathbf{x_{i+1}} &= \mathbf{x_i} + (\mathbf{K_{xi}^T} \cdot \mathbf{S_y^{-1}} \cdot \mathbf{K_{xi}} + \mathbf{S_a^{-1}} + \gamma \mathbf{D})^{-1} \\ &\cdot \{\mathbf{K_{xi}^T} \cdot \mathbf{S_y^{-1}} \cdot [\mathbf{y} - \mathbf{F}(\mathbf{x_i}, \mathbf{b})] + \mathbf{S_a^{-1}} \cdot (\mathbf{x_i} - \mathbf{x_a})\}. \end{aligned} \tag{8}$$

The matrix $\mathbf{K_{xi}}$ is a differential weighting function (or the Jacobian) for each of the retrieval parameters evaluated at $\mathbf{x_i}$. $\mathbf{x_a}$ normally corresponds to the initial guess $\mathbf{x_0}$, $\mathbf{D}$ is a scaling matrix that is usually assumed to be $\mathbf{S_a^{-1}}$, and γ is a Levenberg-Marquardt parameter, which is initially set to 0.0001 in this study. For noisy products such as vertical profiles of mesospheric BrO and HO_2, whose atmospheric densities are small and emissions are weak, the products should be averaged to obtain the information. We use an algorithm of averaging for the noisy products following that of the Aura/MLS (Livesey et al., 2006) (Chapter III).

Characteristics of retrieval results in the standard OEM approach are shown as follows. A contribution matrix $\mathbf{G_y}$, which is the sensitivity of the

retrieved state to the measurement, and an averaging kernel matrix $\mathbf{A}$, which is the sensitivity of the retrieved state to the true state, are defined as follows:

$$\mathbf{G_y} = (\mathbf{K_x^T} \cdot \mathbf{S_y^{-1}} \cdot \mathbf{K_x} + \mathbf{S_a^{-1}})^{-1} \cdot \mathbf{K_x^T} \cdot \mathbf{S_y^{-1}}; \tag{9}$$

$$\mathbf{A} = \mathbf{G_y} \cdot \mathbf{K_x}. \tag{10}$$

In the non-linear case, these matrices are calculated by using the results of the final iteration process. The errors due to the retrieval process are shown as follows: A retrieval covariance matrix $\mathbf{S}$ is defined by

$$\mathbf{S} = (\mathbf{K_x^T S_y^{-1} K_x} + \mathbf{S_a^{-1}})^{-1}. \tag{11}$$

The retrieval precision of the product is defined as the square root of the diagonal elements of $\mathbf{S}$. The retrieval bias due to incorrect knowledge of the forward model parameter is given by the error covariance matrix $\mathbf{S_f}$,

$$\mathbf{S_f} = \mathbf{G_y K_b S_b K_b^T G_y^T}, \tag{12}$$

where $\mathbf{K_b}$ and $\mathbf{S_b}$ are a weighting function matrix and a covariance matrix of $\mathbf{b}$, respectively. In the SMILES, some of these parameters have significant errors compared to $\mathbf{S}$. Therefore, it is important to develop an accurate forward model. In the equation (10) and (11), we ignore $\gamma\mathbf{D}$ term of (8) in accordance with the definition of Rodgers (2000). In the nonlinear case, these matrices are calculated by using the results of the final iteration.

The retrieval process consists of two main parts; the forward model and the inverse model. The inverse model deduces the distributions of geophysical parameters from a given set of calibrated brightness temperatures and

brightness temperatures simulated using the forward model. The forward model simulates the brightness temperatures measured by the SMILES for a given atmospheric state. The output is a convolution of the brightness temperature calculated with atmospheric radiative transfer with the instrumental field of view (FOV) and the spectral response of the AOS.

The brightness temperatures detected by the SMILES antenna is derived by radiative transfer model, which is defined as a transmission process of emissions from atmospheric molecules through the Earth atmosphere. Here, the rays of the emissions are curved by refraction. The emissions from minor components are calculated by line-by-line but the emissions from major components like water vapor are calculated by the model. In the line-by-line calculation, spectroscopic parameters are important for the accuracy of the retrieval process. The convolution with the FOV uses a measured antenna pattern by the ground and includes effects from tilt of SMILES. Since the antenna pattern of SMILES is ellipse, the pattern is changed depending on tilt of SMILES. Furthermore signal from the other sideband of the sideband filter and responce functions of AOS are also considerd in the forward moldel.

The measurement noise of SMILES is very small as I mentioned previously and it is mostly less than 1 K in a single scan. It means that the forward model must provide the most accurate basis for results. The forward model algorithm has to be more accurate than ever before, to make the best of SMILES performance. It also should be required to be fast because of limited computing resources. Therefore to develop the accurate and fast forward

model algorithm is very important issue in the SMILES observation and this study is one of a main part of this thesis.

5 Aim of This Thesis

The various types of atmospheric ozone observation have been performed since 1970's. The trend of the ozone depletion is monitored by worldwide cooperation as previously described. However, the mechanism of the ozone depletion and the prediction of the ozone recovery are still uncertain. SMILES has been planed to improve our understanding of an expected slow recovery of ozone from the depletion, climate change and coupled processes of them by high sensitive measurements of distributions of ozone and ozone-depleting substance.

To maximize the performance of SMILES, an accurate retrieval algorithm must be indispensable because accuracy of the data is determined by both sensitivity of the sensor and accuracy of the retrieval algorithm. Therefore accurate retrieval algorithm has been developed to introduce high-quality vertical profiles of ozone and ozone depleting substance. Furthermore for a requirement of near-real time processing fast retrieval algorithm is also required. The development the retrieval algorithm to balance competing requirements for accuracy and high processing speed is one of a purpose of this thesis. The other purpose of this thesis is estimation for a capability for ozone high-precision retrieval on SMILES observation based on the algorithm and differences from previous measurements are introduced.

The development the fast and accurate retrieval algorithmth for SMILES is described in Chapter II. This Chapter describes the detailed algorithm of the forward model optimized for the SMILES and the validation and perfor-

mance. The study for the capability of ozone observation using SMILES is described in Chapter III. This Chapter refers to the retrieval errors caused by model parameter uncertainties such as a priori profile and uncertainty of the atmospheric temperature, identify the capability for measuring ozone diurnal variation in the upper stratosphere, and present a further improvement of the retrieval algorithm in the lower stratosphere and its random error.

References

Bernath PF, McElroy CT, Abrams MC, Boone CD, Butler M, Camy-Peyret C, Carleer M, Clerbaux C, Coheur PF, Colin R, DeCola P, DeMazie M, Drummond JR, Dufour D, Evans WF, Fast H, Fussen D, Gilbert K, Jennings DE, Llewellyn EJ, Lowe RP, Mahieu E, McConnell JC, McHugh M, McLeod SD, Michaud R, Midwinter C, Nassar R, Nichitiu F, Nowlan C, Rinsland CP, Rochon YJ, Rowlands N, Semeniuk K, Simon P, Skelton R, Sloan JJ, Soucy MA, Strong K, Tremblay P, Turnbull D, Walker K, Walkty I, Wardle DA, Wehrle V, Zander R, Zou J Atmospheric Chemistry Experiment (ACE):Mission overview. Geophys. Res. Lett., 32, L15S01, doi:10.1029/2005GL022386.

Bevilacqua RM, Hoppel K, Hornstein J, Lucke R, Shettle E, Ainsworth T, Debrestian D, Fromm M, Lumpe J, Krigman S, Glaccum W, Olivero J, Clancy RT, Rusch D, Randall C, Dalaudier F, Deniel C, Chassefiere E, Brogniez C, Lenoble J, First results from POAM II: The Dissipation of the 1993 Antarctic Ozone Hole Geophys. Res. Lett.;1995;21;909-912.

Bovensman H, Burrows JP, Buchwitz M, Frerick J, Noël S, Rozanov VV, Chance KV and Goede APH, SCIAMACHY: Mission objectives and measurement modes. J. Atmos.Sci;1999;56(2);127-150

Fischer H and Oelhaf H, Remote sensing of vertical profiles of atmospheric trace constituents with MIPAS limb-emission spectrometers. Appl. Opt;1996;35(16);2787796

Fischer H, Birk M, Blom C, Carli B, Carlotti M, Clarmann T, Delbouille

L, Dudhia A, Ehhalt D, Endemann M, Flaud JM, Gessner R, Kleinert A, Koopman R, Langen J, Lopez-Puertas M, Mosner P, Nett H, Oelhaf H, Perron G, Remedios J, Ridolfi M, Stiller G, Zander R, MIPAS: An instrument for atmospheric chemistry and climate research, ESA Publications Division, Atmospheric Chemistry and Physics;2008;8;8;2188

Froidevaux L, Jiang YB, Lambert A, Livesey NJ, Read WG, Waters JW, Browell EV, Hair JW, Avery MA, McGee TJ, Twigg LW, Sumnicht GK, Jucks KW, Margitan JJ, Sen B, Stachnik RA, Toon GC, Bernath PF, Boone CD, Walker KA, Filipiak MJ, Harwood RS, Fuller RA, Manney GL, Schwartz MJ, Daffer WH, Drouin BJ, Cofield RE, Cuddy DT, Jarnot RF, Knosp BW, Perun VS, Snyder WV, Stek PC, Thurstans RP, Wagner PA, Validation of Aura Microwave Limb Sounder stratospheric ozone measurements. JGR;2008;113;D15S20, doi:10.1029/2007JD008771.

Holton JR, Haynes PH, McIntyre ME, Duglass AR, Rood RB, and Pfster L, Stratosphere-troposphere exchange, Rev. Geophys.;1995;33;403-439.

Kikuchi K,Nishibori T,Ochiai S,Ozeki H, Irimajiri Y,Kasai Y, Koike M,Manabe T, Mizukoshi K, Murayama Y,Nagahama T,Sano T, Sato Ryota,Seta M,Takahashi C. Takayanagi M, Masuko H,Inatani J,Suzuki M, and Shiotani M, Overview and Early Results of the Superconducting Submillimeter-Wave Limb-Emission Sounder (SMILES). JGR;2010;15;D23306;12.

Livesey NJ, Snyder WV, Read WG, Wagner PA, Retrieval algorithms for the EOS Microwave limb sounder (MLS). IEEE-MTT, 44(5), 1144–1155, 2006. doi 10.1109/TGRS.2006.872327

Manabe T, Inatani J, Murk A, Wylde RJ, Seta M, and Martin DH, A New Configuration of Polarization-Rotating Dual-Beam Interferometer for Space Use. IEEE Transactions on Microwave Theory and Techniques;2003;vol.51(6):1696–1704

Manabe T, Fukami T, Nishibori T, Mizukoshi K, and Ochiai S, Measurement and evaluation of submillimeter-wave antenna quasioptical feed system by a phase-retrieval method in the 640-GHz band. IEICE Trans. Commun.; 2008;E91-B(6):1760-1766

Murtagh D, Frisk U, Merino F, Ridal M, Jonsson A, Stegman J, et al., An overview of the previous termOdinnext term atmospheric mission. Can J Phys;2002;80;30919.

NASDA/CRL, JEM/SMILES mission plan, Version 2.1.[Online]. Available: http://smiles.tksc.nasda.go.jp/document/indexe.html; 2002

Ochiai S, Kikuchi K, Nishibori T, Manabe T, Ozeki H, Mizukoshi K, Ohtsubo F, Tsubosaka K, Irimajiri Y, Sato R, and Shiotani M, Performance of JEM/SMILES in orbit. 21th Int'l Symp. Space Terahertz Technol., S8.1, (Oxford, UK), March 2010.

Ozeki H, Kasai Y, Ochiai S, Tsujimaru S, Inatani J, Masuko H, Takahashi C, Mazuray L, and Rosen C, Submillimeter-wave spectroscopic performance of JEM/SMILES. SPIE;2000;4152;255–262.

Read WG, Shippony Z, Schwartz MJ, Livesey NJ, and Snyder WV, The Clear-sky Unpolarized Forward Model for the EOS Aura Microwave Limb Sounder (MLS). IEEE Trans. Geosci. and remote sens;2006;44(5).

Rusch DW, Bevilacqua RM, Randall CE, Lumpe JD, Hoppel KW, Fromm MD, Debrestian DJ, Olivero JJ, Hornstein JS, Guo F, Shettle EP, Validation of POAM II Ozone Measurements with Coincident MLS, HALOE, and SAGE II Observations. JGR;1997;102(23);615–627

Russell JM, Gordley LL, Park JH, Drayson SR, Hesketh DH, Cicerone RJ, Tuck AF, Frederick JE, Harries JE, and Crutzen P, The Halogen Occultation Experiment. JGR; 1993;98;D6;10;777–797.

Rodgers CD, Retrieval of atmospheric temperature and composition from remote measurements of thermal radiation. Rev Geophys and Space Phys;1976;14(4);609-624.

Rodgers CD, Characterization and error analysis of profiles retrieved from remote sounding measurements. JGR;1990;95(5);5587-5595.

Rodgers CD, Inverse methods for atmospheric sounding: theory and practice, Series on atmospheric, oceanic and planetary physics, vol.2. Singapole, World Scentific; 2000

Waters JW, Read WG,Froidevaux L, Jarnot RF, Cofield RE, Flower DA, Lau GK, Pickett HM, Santee ML, Wu DL, Boyles MA, Burke J. R, Lay R. R, Loo M. S, Livesey N. J, Lungu TA, Manney GL, Nakamura LL, Perun VS, Ridenoure BP, Shippony Z, Siegel PH, Thurstans RP, Harwood RS, Pumphrey HC, and Filipiak MJ. The UARS and EOS Microwave Limb Sounder (MLS) experiments. J.Atmos.Sci.;1999;56;194-218.

WMO (World Meteorological Organization), Scientific Assessment of Ozone

Depletion: 2010, Global Ozone Research and Monitoring Project Report No. 52, 516 pp., Geneva, Switzerland, 2011.

Part II
Operational Retrieval Algorithms

6 Introduction

As a part of the ground system for the SMILES, a level 2 data processing system (DPS-L2) has been developed. The retrieval algorithm of the DPS-L2 is based on the standard Optimal Estimation Method (OEM), which is a well-established method used in the field of atmospheric science and has been reported in standard literatures (Rodgers, 1976, 1990, 2000). The DPS-L2 converts the calibrated measurements of brightness temperatures, as referred Level 1B data, which is a processed SMILES data containing calibrated limb emission spectra, into distributions of geophysical parameters along the measurement track of the instrument. The main retrieved geophysical parameters are the vertical profiles of target species and temperature and tangent altitudes. The retrieval process consists of two main parts; the forward model and the inverse model. The forward model simulates the brightness temperatures observed by the SMILES for a given atmospheric state. The output is a convolution of the brightness temperature calculated with atmospheric radiative transfer with the instrumental field of view (FOV) and the spectral response. Since the forward model must provide the most accurate basis for results and be implemented under limited computing resources, the forward model algorithm for the operational code has to be accurate and fast. The inverse model deduces the distributions of geophysical parameters from a

given set of calibrated brightness temperatures and brightness temperatures simulated using the forward model.

This Chapter describes the development of the DPS-L2 along with the details on its algorithm and the algorithm performance. Section 7 presents the framework of the DPS-L2, and Section 8 presents the fundamental retrieval theory. Section 9 gives the detailed algorithm of the forward model optimized for the SMILES. Finally, the validation and performance of this algorithm are reported in Section 10.

7 Framework of DPS-L2

7.1 Ground Data Processing System and Data Flow

The SMILES ground data processing system consists of an Experiment Operating System (EOS) and Data Processing System (DPS). The EOS receives telemetry and sends commands. The DPS is divided into two main units; a data processing system for level 0 and level 1 (DPS-L0/L1) and the DPS-L2.

Downlinked raw data from the SMILES will be received by the DPS-L0/L1 at the User Operation Area (UOA) in the Tsukuba Space Center (TKSC). The DPS-L0/L1 processes the raw data consisting of house keeping (HK) data and science data into level 1B data immediately. The level 1B data are periodically transfered via non-network media to a data server connected to the internet. The DPS-L2 located at the Institute of Space and Astronautical Science (ISAS) automatically receives the level 1B data from the data server through the internet and processes the level 1B data into level 2 data. The level 2 data are converted into the HDF-EOS format and are distributed to users accompanied with the ancillary data on the SMILES

status through a web server. A list of the SMILES data sets is presented in Table 3.

Table 3: JEM/SMILES Data Sets

Data Type	Description
Raw	Unprocessed mission data at binary packets
Level 0	Reconstructed, unprocessed mission data at binary packets
Level 1b	Calibrated instrument radiances and related data
Level 2	Derived geophysical variables at the same resolution and location as the Level 1 source data
Level 3	Variables mapped on uniform space-time grid scales, usually with some completeness and consistency

7.2 Structure of the DPS-L2

Figure 9 shows an overview of the DPS-L2. As the DPS-L2 is designed to be an automatic operating system, a control function of the DPS-L2 transfers the level 1B data and invokes the data processing automatically. Data handling and visualization functions are to support the analysis of the level 2 data and to carry out data checks in real time. These functions are implemented on the Gfdnavi (geophysical fluid data navigator) (Horinouchi et al., 2007). Gfdnavi is a suite of software that facilitates databasing, analysis, data publication, and visualization of geophysical fluid data. The principal function of the DPS-L2 is data processing. In the following sections, we discuss the algorithms of the operational retrieval code (ORC) and their performance.

The DPS-L2 is designed to use a highly portable software and works on a general Linux operating system. The operational environments of the DPS-L2 are summarized in Table 4.

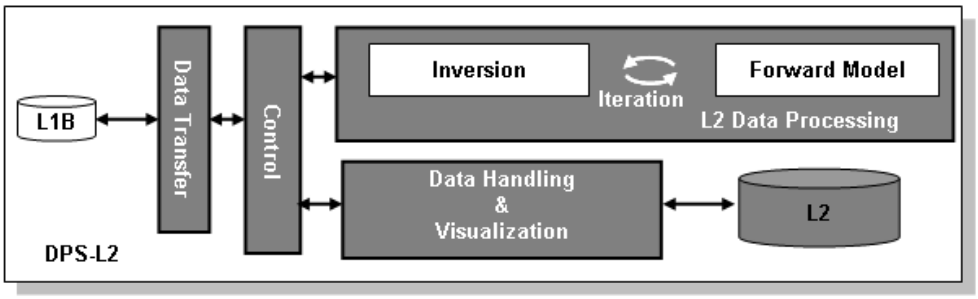

Figure 9: Overview of DPS-L2

Table 4: Operation Environment of DPS-L2

System	Software
Operating System	Linux (kernel: up to 2.6)
Language	gcc (or Intel C++), Ruby, GNU Octave, java
Database	MySQL
Web Application	GFDnavi, ruby on rails

7.3 Requirements for the ORC

There are three significant requirements for developing the ORC, ie. the accuracy, processing speed and portability. The accuracy of the ORC should be sufficiently high to ensure high sensitivity of the SMILES, and is determined by estimation of errors expected in the retrieval. The estimated errors are calculated by the inverse model assuming several parameters such as SMILES radiometric error, FOV characteristics, spectroscopic parameters, and other possible inevitable errors in the forward model. We decided the accuracy of the forward model should be better than 1 % of radiometer noise. Data processing should be carried out in near-real-time (a single scan takes 53 s). Hence, a fast algorithm is required in order to simplify the operations of the system.

For portability, the ORC is written by using two programming languages: C programming language and GNU Octave. GNU Octave is a high-level language, primarily intended for numerical computations (it is mostly compatible with MATLAB). It can be linked with ATLAS (Whaley et al., 2000) to accelerate the processing speed of the system. The forward model is written in C programming language because of its high processing speed and its flexibility to implement considerably complex numerical integration. However, GNU Octave is the most suitable language for the inverse model because the main parts of this model are matrix calculations.

8 Basic Retrieval Algorithm

The retrieval algorithm is based on the OEM applied for atmospheric sounding (Rodgers, 1976, 1990, 2000). The details are in Introduction (Chapter I).

8.1 State Vector x

The components of the state vector $\mathbf{x}$, which is mentioned in Introduction (Chapter I), for the DPS-L2 are as follows:

1. the vertical profiles of the target species concentration in volume mixing ratio;
2. the vertical profiles of atmospheric temperature;
3. the vertical profiles of atmospheric continuum absorption;
4. the offset of the instrument pointing.

The offset of the instrument pointing is a scalar quantity and the other components are vector quantity gridded on the geometrical altitude. The uncertainty of the atmospheric continuum absorption is mainly introduced due to the uncertainty in H_2O distributions. The uncertainties of the instrument pointing are caused by the time synchronous error between the clocks in the SMILES and the ISS, an error in a reference pressure profile, etc.

The standard approach in microwave-limb soundings is to derive the information on the atmospheric temperature and the instrument pointing from oxygen emission lines (Wehr et al., 1998; Livesey et al., 2006). However, since

the SMILES does not observe the oxygen emission lines, these two components can be mainly derived from the ozone emission line at 625.37 GHz (NASDA and CRL, 2002; Verdes et al., 2002). The atmospheric temperature can be retrieved with ozone concentration at a time thanks to the different frequency dependence between weighting functions with respect to ozone and temperature. Most of the information comes from the brightness temperature near the line center where the opacity is sufficiently high to consider the brightness temperature to be independent of ozone concentration but to depend on the atmospheric temperature.

The SMILES can measure the three bands but it measures the two bands simultaneously. Combinations of the simultaneous measurement bands are AB, AC, and BC. For the case of AB, band A and B are processed independently in the launch ready algorithm. However, for the case of AC or BC, the processing should be performed band A (or B) and C, in this order. The reason is that the precision of the retrieved instrument pointing by using of band A (or B) is better than by using band C, and the retrieval result is passed to the retrieval processing of band C.

Our retrieval approach for each band consists of two processes. The first process is the retrieval of the target species in the upper row of Table 1, atmospheric temperature, atmospheric continuum, and the offset of the instrument pointing. These component are retrieved simultaneously. The second process, which is performed after the first processes for the two bands, is the retrieval of the target species in the lower row of Table 1, which are noisy products. These products are retrieved for each product.

We estimate availability of the simultaneous retrieval for the first process. Figure 10 indicates the difference of the incremental error for retrieved ozone between simultaneous (blue line) and sequential retrieval (green line) of ozone and HOCl. The red line is the retrieval precision of ozone, which is the square root of the diagonal elements of $\mathbf{S}$. The simulation setting is that the retrieval altitude step is set to 3 km in 4–70 km region, the measurement tangent altitude step is set to 2 km in 0–80 km region, and the instrument parameters are conformed to Table 5. This simulation is performed on band A using all channels. Here we do not estimate the availability of the channel selection to simplify the retrieval scheme.

The incremental error in ozone retrieval for the simultaneous retrieval is approximately 0.1% in the stratosphere and is almost independent of the a priori. However the incremental error in ozone retrieval for the sequential retrieval depends on the assumptions of profiles of other molecules such as HOCl. For the case that the true profile of HOCl is 100% and 200% greater than the a priori, the incremental errors of ozone are approximately 1.0% and 2.0% in the stratosphere, respectively. Furthermore, the iteration number of the sequential retrieval is larger than that of the simultaneous retrieval. Since this behavior is same as other molecules in the upper row of Table 1, we adopt the simultaneous retrieval for the first process.

9 Optimized Forward Model

9.1 Overview of Forward Model

The forward model calculates the brightness temperatures under the given atmospheric state and also the Jacobians with respect to temperature, the

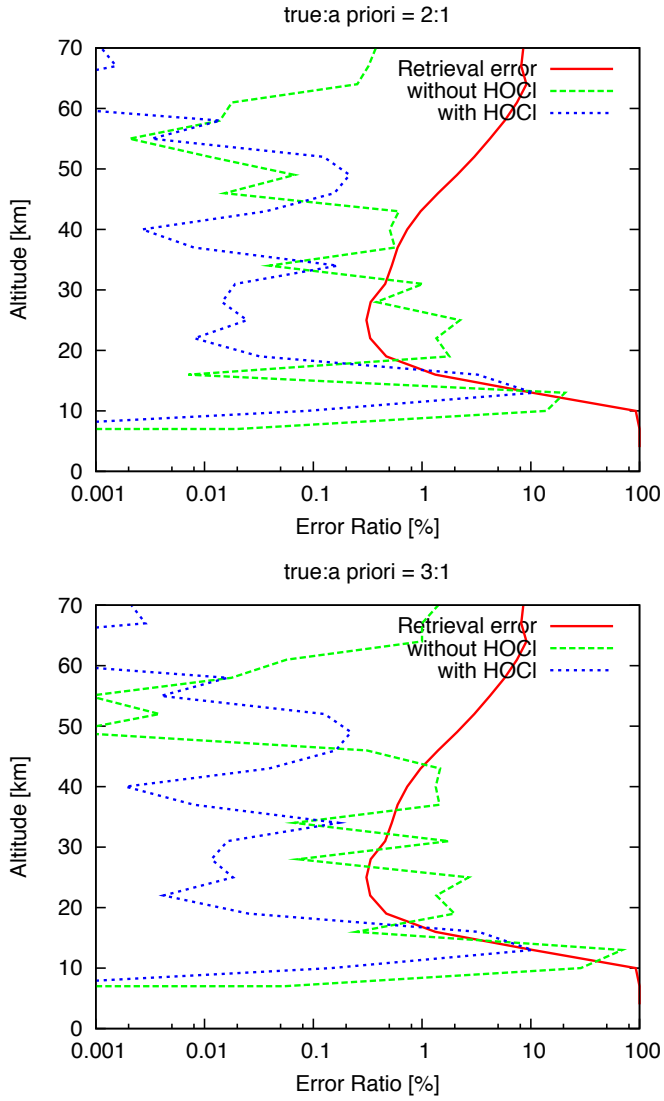

Figure 10: Simultaneous retrieval of ozone and HOCl. The red line indicates the retrieval precision in ozone retrieval, the green line indicates the incremental error in ozone retrieval without HOCl, and the blue line indicates the incremental error in ozone retrieval with HOCl. In all these cases, the true profiles of HOCl are 100% (Right) and 200% (Left) greater than the a priori profile of HOCl. Here, the incremental error is defined as the difference between the true profile and the retrieved profile.

target species concentration, atmospheric continuum, which mainly comes from H_2O, and the offset of the instrument pointing. The forward model carries out the following calculations:

1. ray tracing for the evaluation of the atmospheric state along the limb line-of-sight (LOS) with refraction
2. absorption coefficient calculation for a predefined frequency grid
3. radiative transfer calculation of the single-ray brightness temperature
4. Doppler shift calculation from the ISS velocity, the rotational velocity of the earth, and wind velocity
5. signal convolution with the SMILES antenna FOV considering the inclination of the ISS
6. summation of both sideband signals according to sideband ratio
7. convolution of infinite resolution spectrum and the instrument frequency response

The detailed algorithm is given in the following subsections.

9.2 Radiative Transfer Calculation

9.2.1 Ray Tracing

Refracted ray of limb measurement with arbitrary tangent height is calculated by ray tracing procedures with the following assumptions and conditions. The 1-D radiative transfer calculations described later are defined along the ray calculated here. The earth is assumed to be a sphere whose

radius is curvature radius at the tangent point. The atmospheric refractivity at an altitude z [km] is approximated by

$$n(z) = 1 + 315 \cdot 10^{-6} \cdot \exp(-z/7.35). \tag{13}$$

The variations in the atmosphere are negligible for altitudes above 2 km in the SMILES frequency region (NASDA and CRL, 2002). The step size used in ray tracing is approximately 0.1 km. This step size and the step size used in the path integration in the radiative transfer computation are independent of each other (the step size of a path integration is approximately 1 km).

9.2.2 Absorption Coefficient

For a molecule i with its cross section given by α_i, the absorption coefficient k is given by

$$k(\nu, z) = \sum_i \frac{x_i p}{k_b T} \alpha_i(\nu, z) + k_{\text{cont}}(\nu, z), \tag{14}$$

where z is the altitude, ν is the frequency, x_i is the volume mixing ratio of molecule i, p is pressure, T is temperature, and k_b is the Boltzmann constant. The first term of the right-hand side of Eq. 14 can be calculated line-by-line (LBL) using the JPL Spectral Line Catalog (Pickett et al., 1992), and the second term of the right-hand side of Eq. 14, k_{cont}, is the absorption coefficient of the background continuum for water vapor and dry air (O_2 and N_2) calculated by using Liebe's MPM (Liebe, 1989, 1993). The line shape is described using the Voigt function, which is implemented using a fast algorithm (Kuntz, 1997).

Errors associated with line parameters such as air-broadening parameters and partition functions were estimated by Verdes et al. (Verdes et al.,

2005a,b). According to the papers, partition function errors do not introduce significant error for most of the target species of the SMILES except BrO and the uncertainties in air-broadening parameters lead to comparable errors in the retrieval. These studies on the laboratory measurements of air-broadening parameters have resulted in significant improvements in the retrieval accuracy; therefore, we use the air-broadening parameters of main target species that have already been measured by some research groups (Yamada and Amano, 2005; Oh and Cohen, 1994; Yamada et al., 2003; Drouin, 2004; Goyette et al., 1998; Fischer et al., 2003).

Since the computing cost will be sufficiently reduced by improving algorithm as shown below, k should be recalculated in each scan and each iteration for the accuracy.

9.2.3 Radiative Transfer

Radiative transfer is defined as the process of transmission of the electromagnetic radiation through the atmosphere. The forward model assumes a homogeneous distribution of geophysical parameters along the horizontal. A single-ray radiance at a sensor position s_{s} and at a frequency ν, $I_{\mathrm{p}}(\nu, s_s)$, is given by

$$I_{\mathrm{p}}(\nu, s_{\mathrm{s}}) = I_0 e^{-\tau(\nu, s_{\mathrm{e}}, s_{\mathrm{s}})} + \int_{s_{\mathrm{e}}}^{s_{\mathrm{s}}} B(\nu, T) k(\nu, s) e^{-\tau(\nu, s, s_{\mathrm{s}})} ds. \qquad (15)$$

The first term on the right-hand side of Eq. 15 corresponds to the radiation entering the atmosphere along the direction of the LOS. τ denotes the optical depth between two positions s_1 and s_2 along the LOS and $B(\nu, T)$ is the Planck function, which gives the radiation of a black body at temperature T

and frequency ν:

$$\tau(s_1, s_2) = \int_{s_1}^{s_2} k(\nu, s) ds; \tag{16}$$

$$B(\nu, T) = \frac{2h\nu^3}{c^2} \frac{1}{e^{\frac{h\nu}{k_b T}} - 1}. \tag{17}$$

Here, h is Planck's constant and c is the speed of light. $k(\nu, s)$ is the absorption coefficient at position s along the LOS.

9.2.4 Doppler Shift

The Doppler shift must be taken into account in our forward model. The factors affecting the Doppler shift are the LOS components of the ISS velocity, the rotational velocity of the earth, and wind velocity. The velocity of the ISS is approximately 8 km/s, and the rotational velocity of the earth at the tangent point on the equator is approximately 460 m/s.

Next, we discuss the effect of wind on the Doppler shift. As the maximum velocity of wind in the stratosphere is approximately 100 m/s, there is a Doppler shift of approximately 0.2 MHz. This value is not negligible as compared to the frequency resolution of the acousto-optic spectrometer (AOS), i.e, 1.8 MHz (FWHM). Figure 11 shows the effect of wind on ozone retrieval. Ozone is the molecule that is the most susceptible to these types of effects. The other molecules are not susceptible to these effects, and the incremental errors caused by the Doppler shift are sufficiently small as compared to the retrieval precision. This behavior is also exhibited by other model parameter errors. The red line in Figure 11 indicates the precision of ozone retrieval, and the other lines indicate the incremental error in ozone retrieval for wind velocities equal to 50, 10, and 5 m/s. If the difference of the "true" velocity

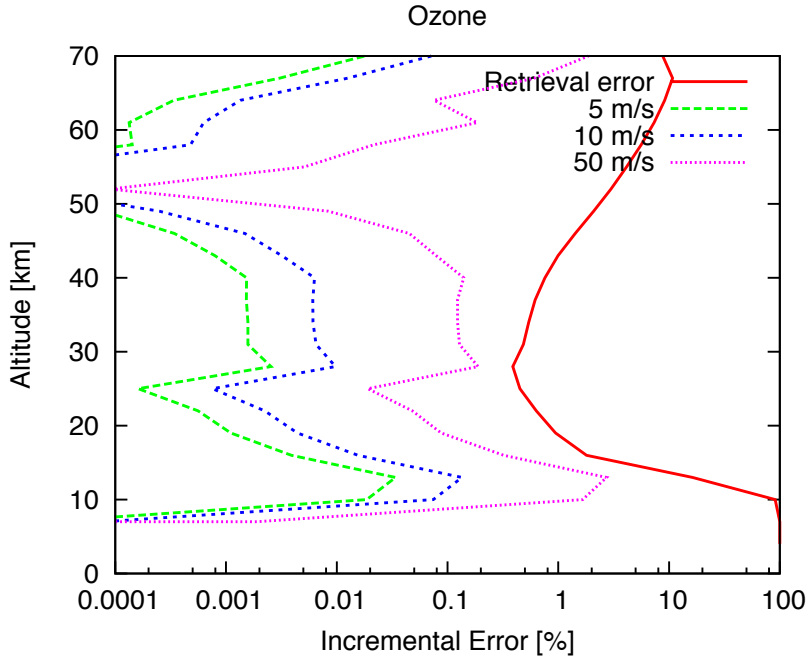

Figure 11: Effect of wind. The red line indicates the retrieval precision of ozone. The other lines indicate the error due to the difference between the reference profile and the true profile of wind.(The wind velocities for the pink, blue, and green profiles are 50, 10, 5 m/s, respectively. The definition of the incremental error is the same as that in Figure 10

and "reference" velocity of wind is less than approximately 10 m/s, the incremental error can be less than 0.005%. This value is sufficiently small as compared to the retrieval precision of ozone. Therefore, we use re-analysis or realtime-analysis data for the reference wind velocity instead of the retrieving the wind speed.

9.3 Accurate Instrument Model for the SMILES

The instrument model is based on the knowledge of the SMILES instrument according to the SMILES missionplan (NASDA and CRL, 2002) and the recent experimental results of the flight model.

9.3.1 FOV Convolution

The FOV of the antenna can be taken into account in the following manner. The brightness temperature convolved by the FOV at its central tangent altitude z_0, $T_{\mathrm{A}}(\nu, z_0)$, is obtained by

$$T_{\mathrm{A}}(\nu, z_0) = \int_{z_{\min}}^{z_{\max}} \bar{P}(z, z_0) \cdot T_{\mathrm{p}}(\nu, z) dz, \tag{18}$$

where $T_{\mathrm{p}}(\nu, z)$ is a single-ray brightness temperature, $\bar{P}(z, z_0)$ is a normalized antenna beam pattern convolved along the horizontal direction, z is the tangent altitude, and $z_{\min}$ and $z_{\max}$ are lower and upper tangent altitudes of field viewed by specified main beam when the antenna is pointing to the tangent altitude of z_0.

It is not improbable that the SMILES antenna scan axis is tilted by 15° from the horizon, which is inclination of the ISS, from the normal inclination. Since the antenna beam of the SMILES has a horizontally flattened elliptical pattern, $\bar{P}(z, z_0)$ depends on the inclination of the antenna scan axis. Figure 12 shows the incremental error in retrieved ozone due to the inclination of the antenna scan axis. If the antenna scan axis inclines by 15°, the incremental error is approximately 1% in the stratosphere, and this value is approximately two times larger than the retrieval precision. Therefore, the effect of the inclination of the antenna scan axis should be taken into consideration in

the derivation of $\bar{P}(z, z_0)$. The antenna beam pattern $P(\tilde{\theta}, \tilde{\psi})$ is measured on the ground with high accuracy, where $\tilde{\theta}$ and $\tilde{\psi}$ are the polar and azimuthal angles respectively with respect to the xyz-axis fixed to the antenna. The y-axis of the antenna is the direction of the main beam. The x-axis of the antenna is perpendicular to the plane formed the y-axis and a longer axis of elliptically shaped main reflector, and is aligned with rotating axis of the antenna that is elevation steerable. The z-axis of the antenna completes the right-handed axes and is positive toward zenith. $P(\tilde{\theta}, \tilde{\psi})$ is measured by a phase-retrieval method (Manabe et al, 2008), which is considered to be effective for measuring and evaluating large-scale submillimeter-wave reflector antennas.

The following equations define θ and ϕ. Those are the polar and azimuthal angles which are exactly the same with $\tilde{\theta}$ and $\tilde{\psi}$ when the x-axis of the antenna becomes perpendicular to the vector toward the center of the earth.

$$\tilde{\theta} = \cos^{-1}\left(-\sin\theta \cdot \cos\psi \cdot \sin\alpha + \cos\theta \cdot \cos\alpha\right), \tag{19}$$

$$\tilde{\psi} = \tan^{-1}\left(\frac{\sin\theta \cdot \sin\psi}{\sin\theta \cdot \cos\psi \cdot \cos\alpha + \cos\theta \cdot \sin\alpha}\right), \tag{20}$$

where α is the angle of the x-axis of the antenna from the local horizontal plane at the tangent point. $P(\tilde{\theta}, \tilde{\psi})$ convolved by θ, $P^*(\theta)$, is

$$P^*(\theta, \alpha) = \int_{\psi_1}^{\psi_2} P(\tilde{\theta}(\theta, \psi, \alpha), \tilde{\psi}(\theta, \psi, \alpha)) \cdot \cos\theta \cdot d\psi. \tag{21}$$

By using the pre-calculated $P^*(\theta, \alpha)$ for every one degree of α, the incremental error for ozone retrieval can be reduced to less than 0.001%. Finally, $\bar{P}(z, z_0)$ is translated from $P^*(\theta)$ by ray tracing with refraction in every operation calculation.

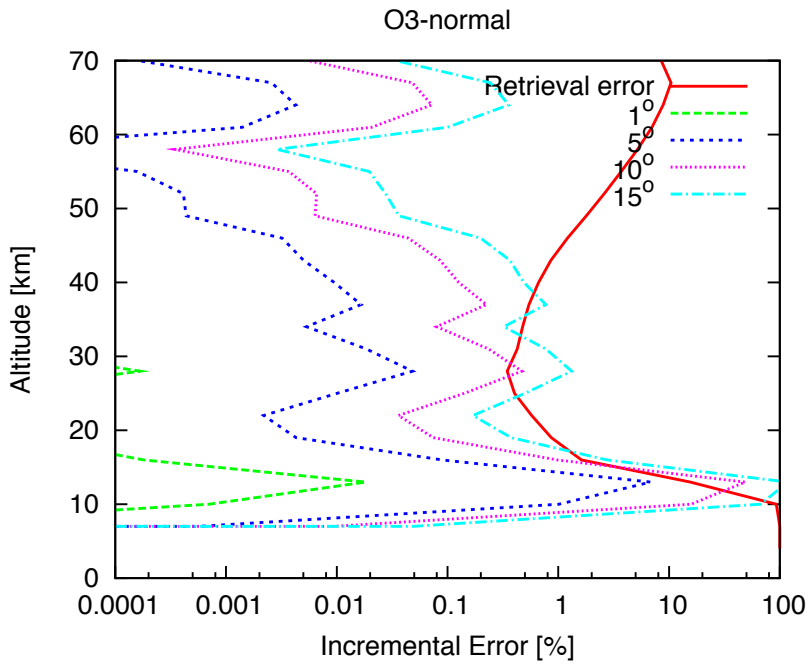

Figure 12: Error due to inclination of antenna scan axis. The red line indicates the retrieval precision of ozone. The other lines indicate the error due to the inclination of the antenna scan axis. The inclinations of the antenna scan axis in the aqua blue, pink, dark blue, and green profiles are 15°, 10°, 5°, and 1°, respectively. The definition of the incremental error is the same as that in Figure 10.

9.3.2 Sideband Ratio

To separate the two sidebands, the SMILES is equipped with a quasi-optical sideband separator in the submillimeter range. The sideband separator of the SMILES, which is a modified Martin-Puplett interferometer (Manabe et al., 2003), can reject the image band signal more than 20 dB in the SMILES measurement bands. Even this rejection ratio, the signal from the image band rises up to approximately 2 K in the lower stratosphere. Since this value is not negligible, the image signal should be calculated in our forward model by using the measured response function. The transmission function, $K^b_{i,j}(\nu, T)$, from the antenna (j=ANT) or cold sky terminator (j=CST) to mixer-i in upper sideband (b=USB) or lower sideband (b=LSB) can be expressed by (19) where $m^b_{i,j}(T)$, $\nu^b_{0i,j}(T)$, $\alpha^b_{i,j}(T)$, are constants those have been experimentally determined based on SMILES ground tests, and i=R or T, j=ANT or CST, b=USB or LSB, T is the temperature of sideband separator.

$$K^{\mathrm{b}}_{i,\mathrm{j}}(\nu, T) = m^b_{i,j}(T)(\nu - \nu^b_{0i,j}(T))^2 + \alpha^b_{i,j}(T). \tag{22}$$

The brightness temperature after the SIS mixer-i, $T_{\mathrm{mix}(i)}(\nu, z_0)$, is given by (NASDA and CRL, 2002)

$$\begin{aligned} T_{\mathrm{mix}(i)}(\nu, z_0) = &\begin{bmatrix} K^{\mathrm{LSB}}_{i,a}(\nu_{\mathrm{LO}} - \nu_{\mathrm{if}}) \\ K^{\mathrm{LSB}}_{i,c}(\nu_{\mathrm{LO}} - \nu_{\mathrm{if}}) \end{bmatrix}^T \cdot \begin{bmatrix} T_{\mathrm{A}}(\nu_{\mathrm{LO}} - \nu_{\mathrm{if}}, z_0) \\ T_{\mathrm{c}}(\nu_{\mathrm{LO}} - \nu_{\mathrm{if}}) \end{bmatrix} \\ &+ \begin{bmatrix} K^{\mathrm{USB}}_{i,a}(\nu_{LO} + \nu_{\mathrm{if}}) \\ K^{\mathrm{USB}}_{i,c}(\nu_{LO} + \nu_{\mathrm{if}}) \end{bmatrix}^T \cdot \begin{bmatrix} T_{\mathrm{A}}(\nu_{\mathrm{LO}} + \nu_{\mathrm{if}}, z_0) \\ T_{\mathrm{c}}(\nu_{\mathrm{LO}} + \nu_{\mathrm{if}}) \end{bmatrix}. \end{aligned}$$

Here, ν_{if} is the intermediate frequency (IF), ν_{LO} is the local frequency, which is 637.32 GHz, and T_A and T_c are the brightness temperature from ANT and CST ports, respectively.

9.3.3 Frequency Response

The SMILES carries two units of AOSs (Ozeki et al., 2000). Each AOS has 1728 channels and covers a bandwidth of approximately 1.2 GHz. Their frequency resolution is approximately 1.8 MHz (FWHM), and the channel separation is typically 0.8 MHz. The central frequency of each channel is well related to channel number by 3rd-order polynomial. The frequency of AOSs are calibrated with a comb generator during every scan. The coefficients of the polynomial are supplied by L1B processing.

According to (NASDA and CRL, 2002) and (Ozeki et al., 2000), the brightness temperatures after the mixer i, $T_{\mathrm{mix}(k)}(\nu, z_0)$, are convolved with the channel response function of the AOS l, $H_{\mathrm{AOS}(l)}(\nu - \nu_j)$, for each channel and the brightness temperature of the jth channel, $T_{\mathrm{AOS}(l)}(\nu_j, z_0)$, is denoted by

$$T_{\mathrm{AOS}(l)}(\nu_j, z_0) = \frac{\int_{\nu_{\min}}^{\nu_{\max}} H_{\mathrm{AOS}(l)}(\nu - \nu_j) \cdot T_{\mathrm{mix}(i)}(\nu, z_0) d\nu}{\int_{\nu_{\min}}^{\nu_{\max}} H_{\mathrm{AOS}(l)}(\nu - \nu_j) d\nu}. \tag{23}$$

Here, ν_j is the central frequency of the jth channel. The channel response function of an AOS is represented by the superposition of some Gaussian profiles, and the channel response function for a channel j is given by

$$H_{\mathrm{AOS}(l)}(\nu - \nu_j) = \sum_{i-1}^{N_i} \frac{A_{i,j}}{w_{i,j}\sqrt{\pi/2}} \cdot \exp\left(-2\frac{(\nu - \nu_j - xc_{i,j})^2}{w_{i,j}^2}\right), \tag{24}$$

where $A_{i,j}$, $w_{i,j}$, and $xc_{i,j}$ are ith parameters of the Gaussian fit. $A_{i,j}$, $w_{i,j}$, and $xc_{i,j}$ depend on each channel of the AOS. The forward model takes in the dependence on the channel based on the measurements.

9.4 Fast Algorithm

9.4.1 Line Selection

Since the absorption coefficient is calculated by LBL, except the background continuum for H_2O and dry air, the computing cost of the absorption coefficient is proportional to the number of absorbing lines. Therefore, it is necessary to select the lines to be calculated as minimum in number as possible to reduce computing cost without sacrificing the accuracy of the calculation. In our estimation, lines that affect more than 5.0e–4 K on the target band should be calculated to satisfy the accuracy. Figure 13 shows the effect of line selection on ozone retrieval. The incremental error due to this line selection (green line) is less than 0.01% in the stratosphere. This value is sufficiently small as compared to the retrieval precision (red line).

The total number of selected lines is approximately 2000 to 3000 per band. Approximately 80% of these lines are outside the bands, and contribution of these lines to the band is not significant because the intensity is relatively low and it does not have steep spectral feature. Therefore, the absorption coefficient of the lines outside the bands can be calculated by using coarse and equally spaced frequency grid (approximately 10 MHz) by spline interpolation. This results in a speed increase of approximately 10.

9.4.2 Frequency Selection

The computing cost of the forward model is proportional to the number of frequency grid points. The interval of the frequency grid around a line center should be suitable for the Doppler width of the line in order to achieve the required accuracy. (Since the Doppler width is approximately 0.4 MHz, the

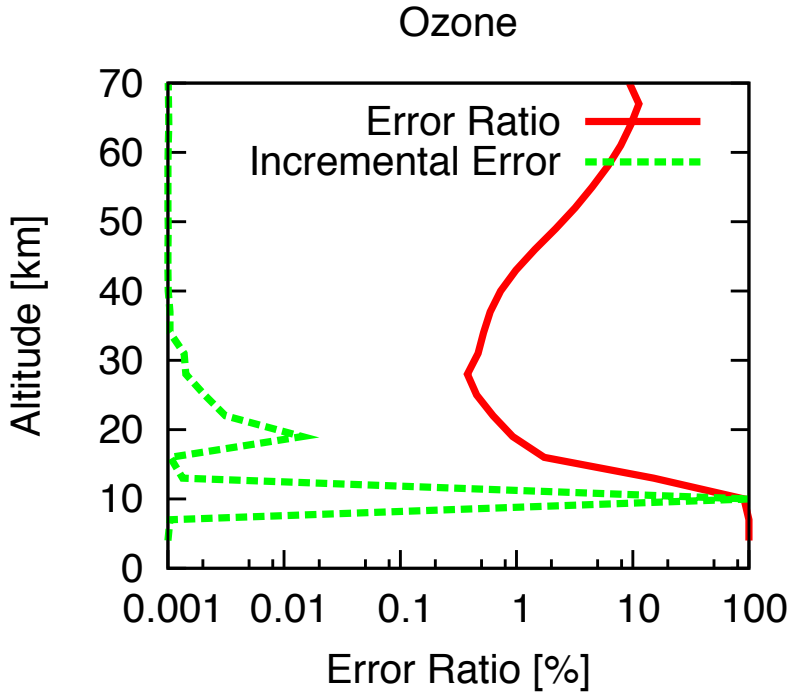

Figure 13: Error due to line selection. The red line is the retrieval precision of ozone, and the green line indicates the incremental error in retrieved ozone due to line selection. The definition of the incremental error is the same as that in Figure 10.

interval of the frequency grid should be less than approximately 0.1 MHz.) On the other hand, the interval can be wide for line wings because the signal level of the line wings is low, and the change is smooth. By optimizing the frequency grid, we can develop a fast algorithm. However, it is difficult to automatically optimize unequally spaced frequency grid.

In our method, the frequency grid is optimized by a sequential process as follows. First, the spectra are calculated by using an initial frequency grid defined by the line centers of a target band and interpolated by a cubic spline function. Next, by comparing the above spectra with the spectra calculated by using the 0.1 MHz equally spaced frequency grid, the maximum difference frequency point is determined. This frequency point is added to the initial frequency grid, and the spectra are calculated by using the new frequency grid. This process is repeated until the maximum difference frequency point is less than 0.001 K.

By using this method, we have found that approximately 900 unequally spaced frequency grid of each band represents a high-accuracy spectrum comparable to the 0.1 MHz equally spaced frequency grid (in this case, we require 12000 points in a band). Using this method, the calculation speed increases by more than a factor of 10. The residual difference of the two frequency sets is less than 0.001 K in all tangent altitude ranges (Figure 14).

10 Results

10.1 Validation of ORC

To validate the ORC, we have compared the various output of the ORC with those of the SMOCO (SMILES observation retrieval code) (NASDA and

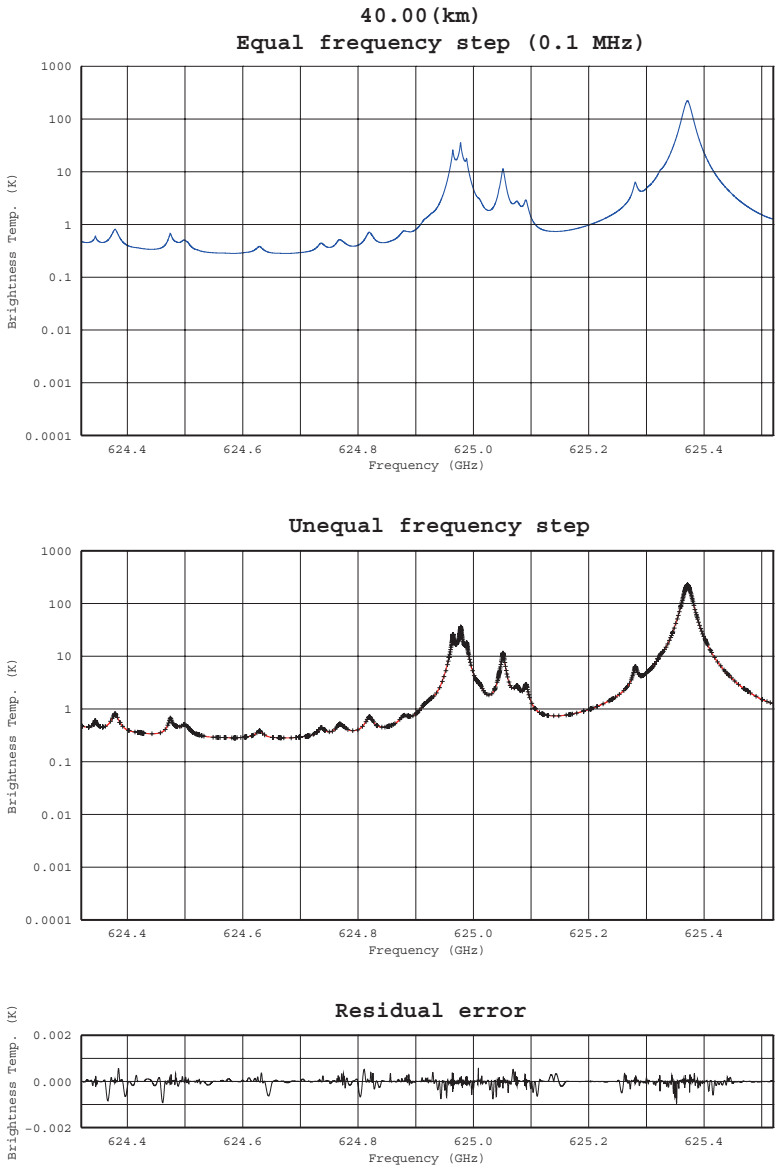

Figure 14: Residual error due to frequency selection. Top: spectrum of band A obtained by using equal frequency step of 0.1 MHz, middle: spectrum of band A obtained by using unequal frequency steps produced by our algorithm, and bottom: residual error.

CRL, 2002; Kasai et al., 2008). The SMOCO is a simulator that includes the radiative transfer calculation for simulating atmospheric sounding in the millimeter and submillimeter wavelength range. The SMOCO has been compared with several models such as ARTS (Bühler et al., 2005), MOLIERE (Ueban et al., 2004), and MAES (Ochiai et al., 2000), and its accuracy has been verified (Melsheimer et al., 2005). Figure 15 shows the error ratio of the absorption coefficient for the ozone line at 625.37 GHz under the same atmospheric conditions. The error ratio is less than 0.03%. This difference can be attributed to the difference in the line shape model of the Voigt profile. There are no fundamental problems in the absorption coefficient calculation. Next, we have compared the monochromatic brightness temperature of the limb emission from the ozone line obtained using the ORC and SMOCO. In this case, we have ignored the effects of the instruments such as the antenna and AOSs. Figure 16 shows the error of the brightness temperature obtained using the ORC and the SMOCO. The error in both cases is less than 0.2% (less than 0.05 K error in absolute value). The largest difference is appeared at 10 km and this altitude range corresponds to the tropopause. Around the tropopause, the gradient of absorption with respect to altitude is so steep that small difference of models tends to be amplified. We concluded that this level of difference is acceptable in the retrieval for the stratosphere, which is our target and that there are no fundamental problems encountered in the radiative transfer calculation.

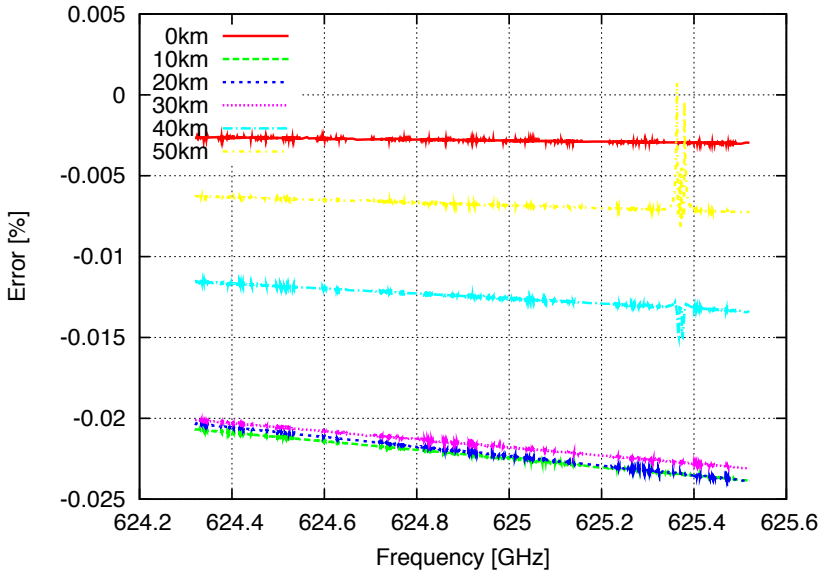

Figure 15: Residual error of absorption coefficients at 0 km (red), 10 km (green), 20 km (blue), 30 km (pink), 40 km (aqua), and 50 km (yellow). The residual error is defined by (SMOCO-ORC)/SMOCO.

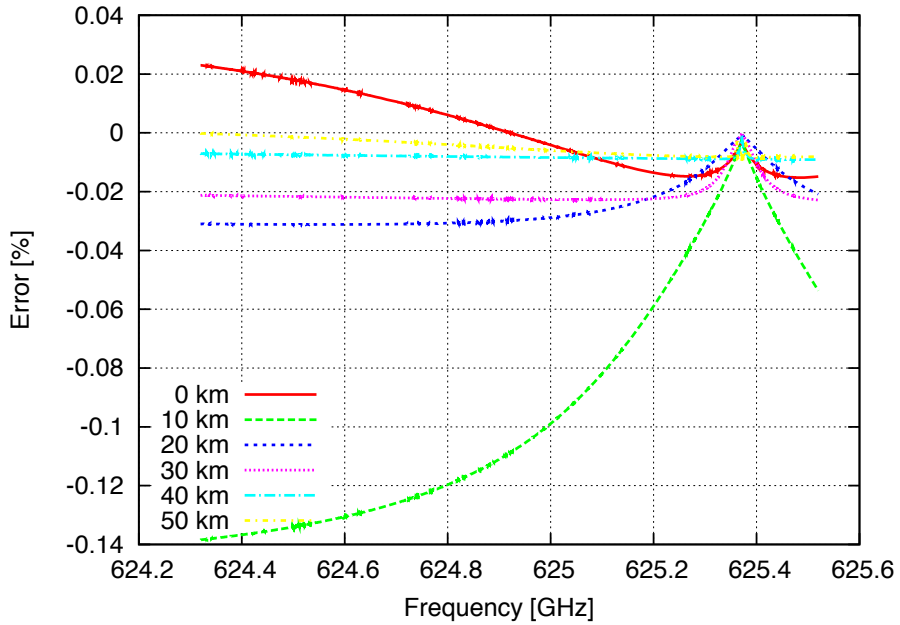

Figure 16: Residual error of brightness temperature. Legends are the same as those used in Figure 15

10.2 Error Budget

Here, we focus on the retrieval errors in the ozone profile in order to discuss the error budgets, because ozone is the representative species of the SMILES mission. The main error budgets are

- Smoothing error
- Retrieval noise
- Forward model parameter errors
  - In sufficient information on the profiles of nonretrieved parameters
  - Approximations of the instrument functions
  - Incorrect input parameters
  - Approximations of the fast algorithm.

The retrieval noise can be evaluated from the covariance of measurements, $\mathbf{S_y}$. In case of radiometer whose spectral channels are almost uncorrelated each other, $\mathbf{S_y}$ is a diagonal matrix and each diagonal element, σ_y, is calculated by

$$\sigma_y = \frac{T_{sys} + T_A}{\sqrt{B\tau}}, \tag{25}$$

where T_A is the measurement brightness temperature, T_{sys} is the system noise (500 K), B is the noise band width (2.5 MHz), and τ is the integration time (0.5 s). σ_y is one order smaller than that of existing satellite sensors, and the error of ozone retrieval mainly due to retrieval noise is less than 0.5% at 30 km (Figure 19). This estimation is based on the standard mid-latitude profile, and the standard deviation of a priori profile is assumed to

be 100% for all species. Because of the high sensitivity, the forward model parameter errors cannot be considered to be negligible as compared to the retrieval noise. In some cases, the forward model parameters are the most significant errors. Since most of the forward model parameter errors are systematic errors, they affect the accuracy of the retrieved profiles. We have studied the technique to reduce these errors and have developed an accurate algorithm on the basis of these studies. As we have showed in Section 8.1, this effect can be reduced to retrieve all species whose signal is larger than a few kelvins (species in the upper row of Table 1). The instrument functions have been designed to model the measurements, which have been carried out meticulously for each module of the SMILES on the ground by the hardware team of the SMILES. In the determination of the attitude of the ISS for the antenna beam pattern, the error due to FOV convolution is minimized and assumed to be negligible. Basic studies on the incorrect input parameters such as spectroscopic parameters have been carried out by the University of Bremen. However, further studies have to be carried out after the launch.

Although these calculations increase the computing cost since importance is given to accuracy instead of the computing cost, the computing cost can be reduced by using the fast algorithm given in Section 9.4. The speed of calculation using this algorithm is nearly ten times higher than that of the normal algorithms such as the line selection algorithm and frequency selection algorithm without degradation of the accuracy. The accuracy of the spectra of the stratospheric minor species is up to 0.01 K (1% of the system noise).

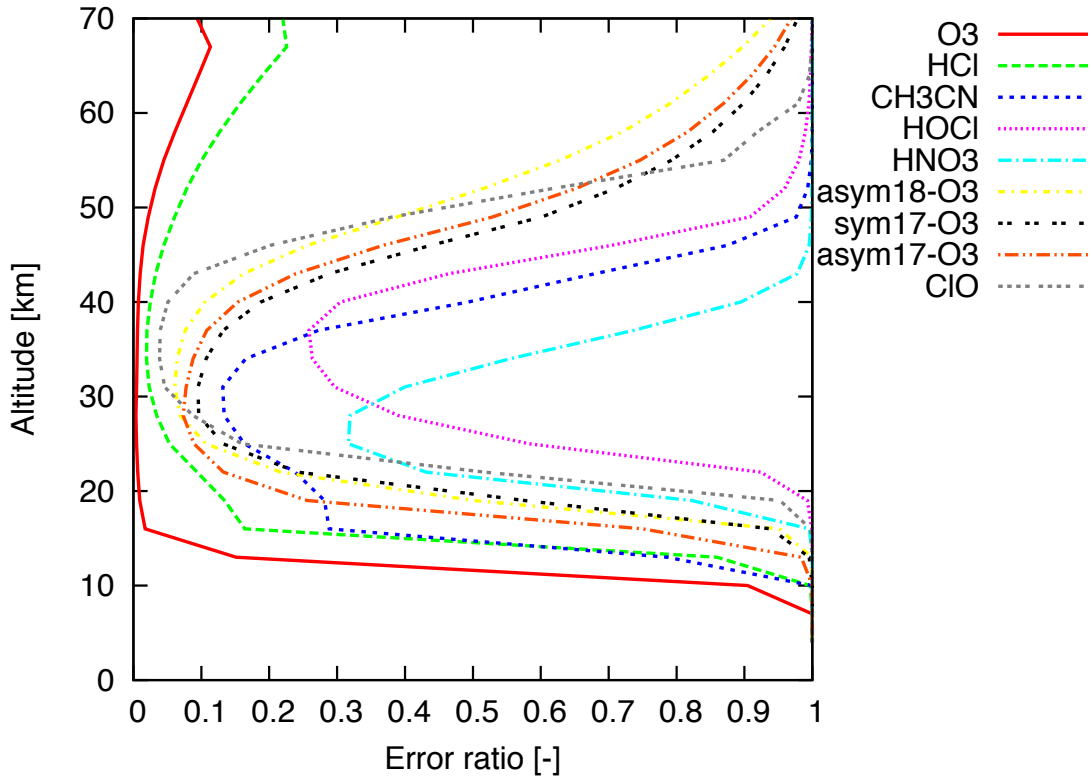

Figure 17: Retrieval precision of target species that can be retrieved from single-scan data.

10.3 Algorithm Performance and Hardware System

The algorithm performance has been tested using a 3.16–GHz Quad-Core Intel Xeon processor. The test was performed using the single-scan data of band A, which requires the longest processing time among the three SMILES bands. In band A, seven molecules (Table 1), temperature, and the offset of the tangent altitude are retrieved simultaneously, while in bands B and C, only four molecules (Table 1) are retrieved simultaneously. Hence, the processing time of bands B and C is approximately 30% lesser than that of band A. We have used the Intel C++ compiler and the 64-bit linux OS because the Intel C++ compiler is 2.5 times faster than gcc, and the 64-bit linux OS is 1.5 times faster than a 32 bit OS. The total processing time of the forward and inverse models without iteration is 56 s per core. To assume four iterations, the total processing time for a single scan, which has two bands, is performed 1 min per core with 8 parallel processing.

According to this estimation, we have designed the hardware system configuration suitable for the DPS-L2. Assuming three times redundancy and approximately four times iterations, the runtime processing is performed using five servers that have two Quad-Core processors compatible with the 3.16-GHz Quad-Core Intel Xeon on the safe side. Further, two or three small servers are required to process the level 2 data, to manage the database, and to distribute the level 2 data along with the information of the SMILES to users. The hardware system configuration is very compact, and it is convenient to operate and maintain the system.

11 Summary

We have developed a launch ready retrieval algorithm. This algorithm is based on a modification of the Gauss-Newton method called the Levenberg-Marquardt method so that it can support nonlinear cases also. The most important objective of this study is how to realize a highly accurate forward model. As shown in Section 10, this retrieval algorithm can keep the forward model parameter errors at a low level compared to the retrieval precision. Furthermore, the algorithm is sufficiently fast to process the single-scan data within 1 min with 8 parallel processing. Using this algorithm, we expect to obtain data with high accuracy compared to the data obtained using the existing sensors in orbit.

References

Baron P, Merino F, and Murtagh D, Simultaneous retrievals of temperature and volume mixing ratio constituents from non-oxygen Odin submillimeter bands. Opt.;2001;40(33);6102- • 110.

arts Bühler SA, Eriksson P, Kuhn T, Engeln A, and Verdes C, ARTS, the atmospheric radiative transfer simulator. JQSRT;2005;91(1);65–93.

Drouin BJ, Temperature dependent pressure induced lineshape of the HCl J = 1 ← 0 rotational transition in nitrogen and oxygen. JQSRT;2004;83(3–4);321–331.

Fischer J, Gamache RR, Goldman A, Rothman LS, and Perrin A, Total internal partition sums for molecular species in the 2000 edition of the HITRAN database. JQSRT;2003;82(1–4);401- • 12.

Goyette MT, Cohen EA, and Lucia CF, Pressure broadening of HNO3 by N2 and O2: an intercomparison of results in the millimeter wave region. JQSRT;1998;60(1);77–84.

Horinouchi T, Nishizawa S, Watanabe C, Morikawa Y, Koshiro T, Ishiwatari M, Hayashi Y, and Shiotani M, Development of Gfdnavi: a new desktop/server tool for geophysical fluid database, analysis, and visualization. Proceedings of Data Engineering Workshop 2007;D2-8;8 (in Japanese)

Irimajiri Y, Noguchi T, Shi SC, Manabe T, Ochiai S, and Masuko H, A 650-GHz band SIS receiver for balloon-borne limb-emission sounder. Int. J. Infr. Millimeter Waves;2000;21(4);519–526.

Irimajiri Y, Manabe T, Ochiai S, Masuko H, Yamagami T, Saito Y, Izutsu N, Kawasaki T, Namiki M, and Murata I, BSMILES–A Balloon-Borne Superconducting Sub-Millimeter-Wave Limb-Emission Sounder for statrospheric measurements. IEEE Trans. on Geoscience and Remote Sensing;2006;3(1).

Kasai Y, Urban J, Takahashi C, Hoshino S, Takahashi K, Inatani J, Shiotani M, and Masuko H, Stratospheric ozone isotope enrichment studied by submillimeter wave heterodyne radiometry: the observation capabilities of SMILES. IEEE Trans. on Geoscience and Remote Sensing;2006;3(1).

Kasai Y, Ochiai S, Super-Conductive Submillimeter-Wave Limb Emission Sounder Onboard International Space Station: Algorithm Development of for the Data Processing. Jounal of The National Institute of Information and Communications Technology;2008;55(1),97–108

Kuntz M, A new implementation of the Humlicek algorithm for the calculation of the Voigt profile function. JQSRT;1997;57(6);819–824.

Levenberg K, A method for the solution of certain problems in least squares. Q. J. Appl. Math.;1944;2;164–168.

Liebe HJ, MPM–an atmospheric millimeter-wave propagation model. Int. J. Inf. Millim. Waves;1989;10(6):631–650.

Liebe HJ, Hufford G, and Cotton M, Propagation modeling of moist air and suspended water/ice articles at frequencies below 1000 GHz. AGARD 52nd Specialist Meeting of the Electromagnetic Wave Propagation Panel, Palma De Mallorca, Spain, 1993.

Livesey NJ, Snyder WV, Read WG, Wagner PA, Retrieval algorithms for the EOS Microwave limb sounder (MLS). IEEE-MTT, 44(5), 1144–1155, 2006. doi 10.1109/TGRS.2006.872327

Manabe T, Inatani J, Murk A, Wylde RJ, Seta M, and Martin DH, A New Configuration of Polarization-Rotating Dual-Beam Interferometer for Space Use. IEEE Transactions on Microwave Theory and Techniques;2003;vol.51(6):1696–1704

Manabe T, Fukami T, Nishibori T, Mizukoshi K, and Ochiai S, Measurement and evaluation of submillimeter-wave antenna quasioptical feed system by a phase-retrieval method in the 640-GHz band. IEICE Trans. Commun.; 2008;E91-B(6):1760-1766

Marquardt DW, An algorithm for the least-squares estimation of nonlinear parameters SIAM J. Appl. Math.;1963;11(2);431–441.

Melsheimer C, Verdes C, Bühler S, Emde C, Eriksson P, Ichizawa S, John V, Kasai Y, Kopp G, Koulev N, Kuhn T, Lemke O, Ochiai S, Schreier F, Sreerekha T, Takahashi C, Tsujimaru S, and Urban J. Intercomparison of general purpose clear-sky atmospheric radiative transfer models for the millimeter and sub-millimeter spectral range. Radio Sci.;2005;40;R51007,doi:10.1029/2004RS003110.

NASDA/CRL, JEM/SMILES mission plan, Version 2.1. [Online]. Available: http://smiles.tksc.nasda.go.jp/document/indexe.html; 2002.

Ochiai S, Irimajiri Y, and Masuko H, 270 GHz SIS radiometer for stratospheric ClO observation. SPIE;2000;4152;372–379.

Ochiai S, Tsujimaru S, Irimajiri Y, and Manabe T, Stratospheric ozone and clo measurement using balloon-borne submillimeter limb sounder. IEEE Trans. on Geoscience and Remote Sensing;2004;8.

Oh J and Cohen EA, Pressure broadening of ClO by N2 and O2 near 204 and 649 GHz and new frequency measurements between 632 and 725 GHz. JQSRT;1994;54;151–156.

Ozeki H, Kasai Y, Ochiai S, Tsujimaru S, Inatani J, Masuko H, Takahashi C, Mazuray L, and Rosen C, Submillimeter-wave spectroscopic performance of JEM/SMILES. SPIE;2000;4152;255–262.

Pickett HM, Poynter RL, and Cohen EA, Submillimeter, millimeter, and microwave spectral line catalogue. Technical Report JPL Publication 80–23, Rev.3, JPL, 1992.

Read WG, Shippony Z, Schwartz MJ, Livesey NJ, and Snyder WV, The clear-sky unpolarized forward model for the EOS Aura Microwave Limb Sounder (MLS). IEEE Trans. Geoscience and Remote sensing;2006;44(5).

Rodgers CD, Retrieval of atmospheric temperature and composition from remote measurements of thermal radiation. Rev. Geophys. and Space Phys.;1976;14(4);609–624.

Rodgers CD, Characterization and error analysis of profiles retrieved from remote sounding measurements. JGR;1990;95(5);5587–5595.

Rodgers CD, Inverse methods for atmospheric sounding: theory and practice, Series on atmospheric, oceanic and planetary physics, vol.2. Singapole, World Scentific; 2000

Urban J, Baron P, Lautié N, Dassas K, Schneider N, Ricaud P, and La Noë J, Moliere (v5): A versatile forward- and inversion model for the millimeter and sub-millimeter wavelength range. JQSRT;2004;83(3–4);529–554.

Verdes C, Bühler SA, Engeln A, Kuhn T, Kuenzi K, Eriksson P, and Sinnhuber BM, Pointing and Temperature Retrieval from Millimeter/Sub-Millimeter Limb Soundings. JGR;2002;107(D16);4299;doi:10.1029/2001JD000777.

Verdes CL, Bühler SA, Perrinb A, Flaudb JM, Demaisonc J, Wlodarczakc G, Colmontc JM, Cazzolid G, and Puzzarinid C, A sensitivity study on spectroscopic parameter accuracies for a mm/sub-mm limb sounder instrument. J. Mol. Spectrosc;2005;229(2);266- • 75.

Verdes C, Engeln A, and Bühler SA, Partition function data and impact on retrieval quality for a mm/sub-mm limb sounder. JQSRT;2005;90(2);217- • 38.

Yamada M, Kobayashi M, Habara H, Amano T, and Drouin BJ, Submillimeter-wave measurements of the pressure broadening of BrO. JQSRT;2003;82(1–4);391–399.

Yamada M and Amano T, Pressure broadening measurements of submillimeter-wave lines of O3. JQSRT;2005;95(2);221-230.

Waters JW, Read WG, Froidevaux L, Jarnot RF, Cofield RE, Flower DA, Lau GK, Pickett HM, Santee ML, Wu DL, Boyles MA, Burke JR, Lay RR, Loo MS, Livesey NJ, Lungu TA, Manney GL, Nakamura LL, Perun VS, Ridenoure BP, Shippony Z, Siegel PH, Thurstans RP, Harwood RS,

Pumphrey HC, and Filipiak MJ, The UARS and EOS Microwave Limb Sounder (MLS) experiments. J. Atmos. Sci.;1999;56;194–218.

Wehr T, Bühler SA, Englen A, Kunzi K, and Langen J, Retrieval of spectroscopic temperatures from space borne microwave limb sounding measurements. J. Geophys. Res.;1998;103;25,997–26,006.

Whaley RC, Petitet A, and Dongarra JJ, Automated empirical optimizations of software and the ATLAS project. Parallel Computing;2000;27(1–2);3–35.

Part III
Capability for Ozone retrieval

12 Introduction

In this Chapter, we refer to theoretical evaluations for the random error and the systematic error of O_3 vertical profiles based on the launch-ready retrieval algorithm developed for the operational data processing system of SMILES (Takahashi et al., 2009). Since the O_3 emission line at 625.37 GHz is the most intense emission line within the SMILES measurement bands and it affects the retrieval of the other target species measured together, it is important to evaluate the O_3 retrieval so that other species can be retrieved accurately.

The altitude region where SMILES can detect O_3 has been estimated between 20 km and 60 km (NASDA and CRL, 2002) but the altitude regions below 20 km and above 60 km have not been adequately assessed to determine the quality of O_3 retrievals possible in these regions. Therefore, we will determine the measurable altitude region more strictly here. It is difficult to retrieve the O_3 profiles in the low- and high-altitude regions. In the low-altitude region, the uncertainty of the continuum emission by water vapour and scattering by clouds reduces the accuracy of the retrieved O_3 profiles and in the high-altitude region the random error becomes worse with decreasing abundance of O_3. It is important to determine the O_3 distribution in these low- and high-altitude regions to improve understanding of the ozone chemistry.

The launch-ready retrieval algorithm is based on the optimal estimation method (OEM), which is discussed in Section 8. Section 13 provides

an overview of SMILES, including the SMILES measurement technique and Section 14 provides O_3 retrieval results. Section 15 refers to the retrieval errors caused by model parameter uncertainties such as a priori profile and uncertainty of the atmospheric temperature. In Section 16, we identify the capability for measuring O_3 diurnal variation in the upper stratosphere. Finally, we present a further improvement of the retrieval algorithm in the lower stratosphere and its random error in Section 17.

13 O_3 Measurements with the JEM/SMILES

SMILES measures the submillimeter-wave limb emission from the atmospheric minor species, such as O_3, ClO, HCl, HNO_3, HOCl, CH_3CN, HO_2, BrO and O_3 isotopes. The nominal altitude coverage is 10–60 km while the altitude coverage of tangent altitude by the antenna scanning is typically between -10 km and 100 km. The most unique characteristics of the SMILES measurements is their high-sensitivity to atmospheric limb emission in the submillimeter-wave range thanks to the 4-K cooled SIS mixers. Overall system noise temperature of SMILES was designed to be less than 700 K and after the launch it was found to be less than 400 K (Kikuchi et al., 2010). It is better than previous millimeter-submillimeter limb measurements from satellites such as Aura/MLS (Read et al., 2006), whose system noise temperature is approximately 10,000 K at a 600 GHz frequency range, and Odin/SMR (Murtagh et al., 2002), whose system noise temperature is approximately 3,000 K. The relationship between the system noise temperature $T_{\rm sys}(\nu)$ and

the noise level of the brightness temperature $\sigma(\nu, z_T)$ is

$$\sigma(\nu, z_T) = \frac{T_{\mathrm{sys}}(\nu) + T_{\mathrm{A}}(\nu, z_T)}{\sqrt{B\tau}}, \tag{26}$$

where $T_{\mathrm{A}}(\nu, z_T)$ is the measurement brightness temperature at a frequency ν and a tangent altitude z_T, B is the noise bandwidth (1.5 to 2.0 MHz), and τ is the integration time (0.5 s). The noise level of the brightness temperature of SMILES for a single scan is approximately 0.7 K.

SMILES measures three frequency bands: band A (624.32–625.52 GHz), band B (625.12–626.32 GHz) and band C (649.12–650.32 GHz). Only two of them are measured simultaneously. Figure 18 shows measured spectra in the mid-latitudes atmosphere at approximately 10 (red line), 30 (green line) and 50 km (blue line) tangent altitude for each band. The brightest emission line in the SMILES measurement bands is the O_3 emission line at 625.37 GHz in bands A and B. The spectra at 30 km tangent altitude indicate that SMILES is a suitable instrument to measure the target species in the middle stratosphere. The spectra at 10 km tangent altitude are almost saturated by water vapor continuum whereas at 50 km tangent altitude emission lines of the most of target species (except O_3 and HCl) are less than the noise level of SMILES (approximately 1 K). Therefore, we need further improvements for the retrieval algorithm in these altitude regions. Detailed estimations for O_3 retrieval in these altitude regions are in Section 16 and 17.

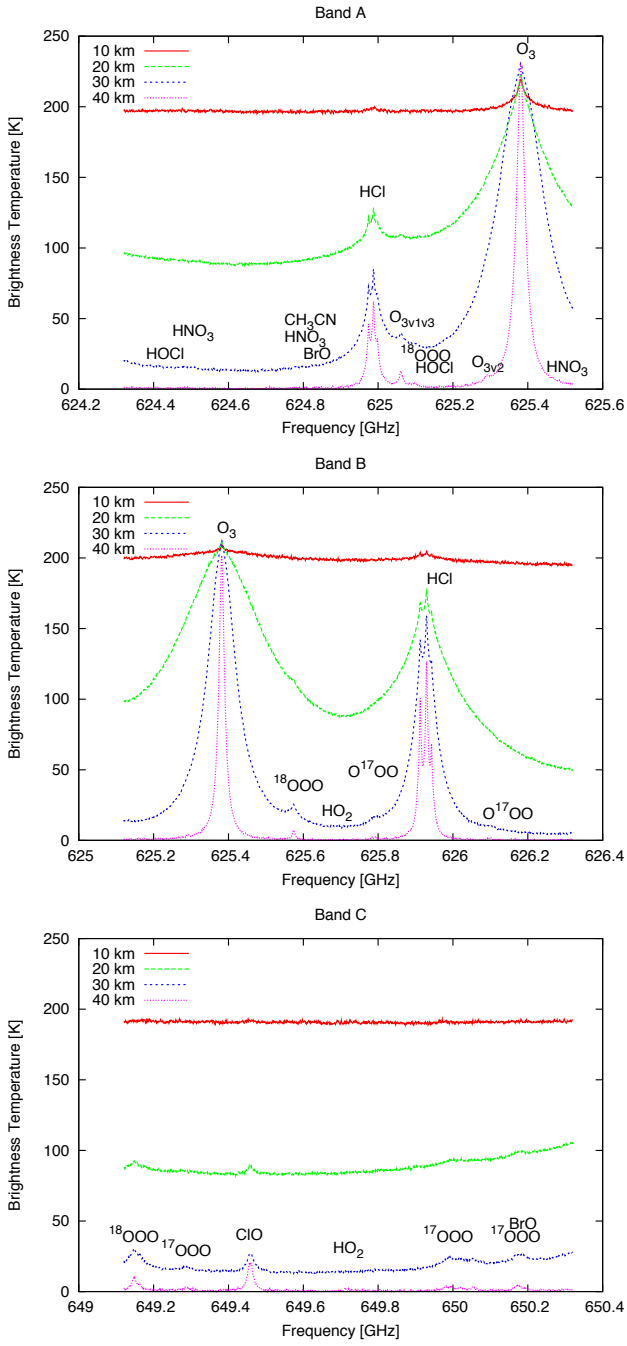

Figure 18: Measured spectra by SMILES. There are three bands; band A (top), B (middle) and C (bottom) at approximately 10 km (red/solid line), 20 km (green/dashed line), 30 km (blue/dotted line), and 40 km (pink/fine dotted line).

14 Retrieval Results

14.1 Setup Conditions

The retrieval algorithm is based on the OEM applied for atmospheric sounding (Rodgers, 1976, 1990, 2000). The details are in Introduction (Chapter I). The species included in the simulation are O_3, HCl, ClO, HOCl, HNO_3, CH_3CN, HO_2, BrO and H_2O. Spectroscopic line parameters for those species are taken from the JPL catalog (Pickett et al., 1992) and H_2O background continua is calculated by Liebe's model (Liebe, 1989). The retrieval parameters are the vertical profiles of the mixing ratio for these species, the atmospheric temperature profile and a pointing offset. The profiles used in this simulation are from the US standard atmosphere. Standard deviations of the a priori profiles for the species, temperature and pointing offset are 100% of the a priori profiles, 5 K in the entire altitude range, and 5 km (as estimated for the uncertainty of the ISS attitude (NASDA and CRL, 2002)), respectively.

The measured tangent altitude region used in the retrieval is 0–80 km and the altitude grid step is approximately 2 km width. The vertical grid step is set to 3 km in the 4–70 km region for all retrieval parameters. Other instrument parameters are listed in Table 5. Standard deviations of the measurement brightness temperature (the square root of the diagonal elements of $\mathbf{S_y}$) are defined by the equation 26.

14.2 Random Error and Vertical Resolution

We estimate the random error of the retrieved O_3 profiles under clear sky conditions by using single-scan spectral data of band A, because band A pro-

Table 5: JEM/SMILES design specifications

System Parameter	Description
Frequency bands	Band A (624.3–625.5 GHz)
	Band B (625.1–626.3 GHz)
	Band C (649.1–650.3 GHz)
System noise temperature	Less than 700 K
Instrumental vertical resolution	3.5–4.1 km (nominal)
Frequency resolution	1.8 MHz (FWHM)
Channel separation	0.8 MHz channel
Integration time	0.5 s for each observation point
Altitude range	10–60 km (nominal)
Global coverage	38°S–65°N (nominal)
Antenna scan period	53 s/scan
Horizontal sampling interval	360 km (in orbital direction)
Orbit period	90 min.

vides the highest sensitivity for the stratospheric O_3. The red line in Figure 19 is the random error of O_3, which is the square root of diagonal elements of $\mathbf{S}$, in the case of $T_{\rm sys} = 500$ K (typical for SMILES observations). The green line is the random error of O_3 in the case of $T_{\rm sys} = 5000$ K (comparable with previous submillimeter or millimeter radiometers). In fact, according to Livesey et al. (2007) the random error of O_3 measured by the Aura/MLS is estimated 2% at approximately 25 km and 5% in the altitude range from approximately 20 to 40 km. The best random error of O_3 by using the SMILES measurement is approximately 0.4% at 28 km altitude. The random error is better than 10% in the altitude region from 13 to 70 km, 5% in the altitude region from 15 to 55 km and 2% in the altitude region from 16 to 48 km. The random error of O_3 is approximately one order of magnitude better than that from previous submillimeter or millimeter radiometers. Here, we only discuss the random error, but systematic errors caused by the uncertainty

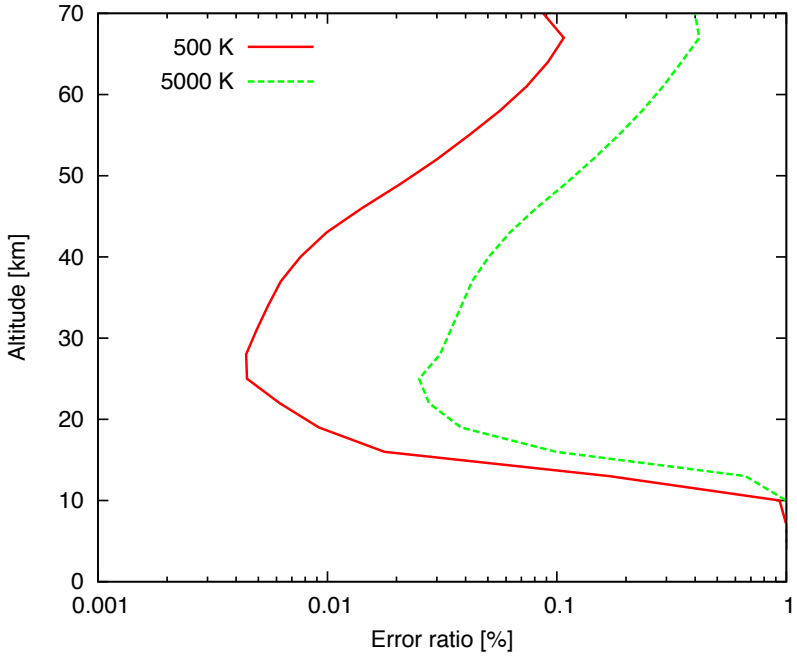

Figure 19: The solid red line and dashed green line indicate the random error for the system noise of 500 K and 5000 K, respectively.

of the model parameters are also important in the discussion of the product quality. These errors will be estimated in Section 15.

Next, we refer to the vertical resolution of the retrieved O_3 profile. The averaging kernels of O_3 for the bands A, B and C are shown in Figure 20. The full width at half maximum (FWHM) of the averaging kernel for each altitude indicates the vertical resolution of the retrieved O_3 profiles. Since the retrieval altitude grid step is 3 km in the retrieval, the minimum altitude resolution is 3 km in this case. The vertical resolution of 3 km is achieved from 10 to 70 km in the case of the bands A and B and 10 to 40 km in the case of band C.

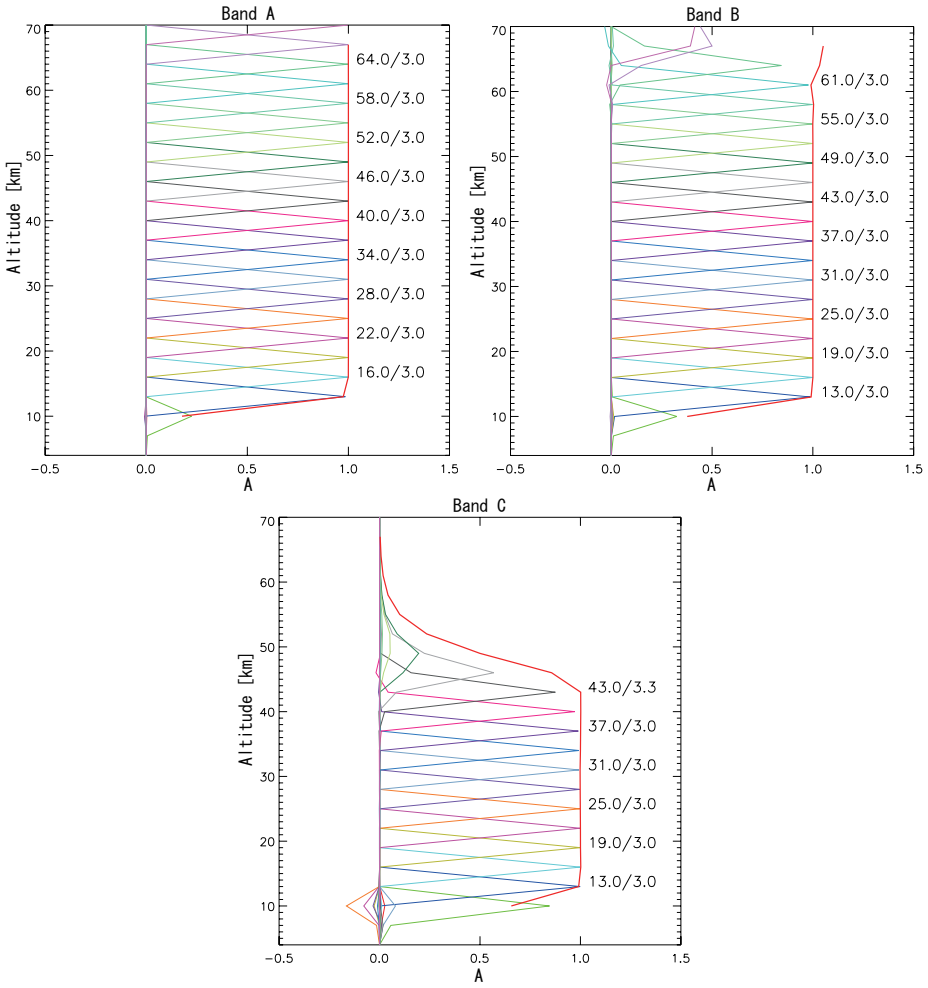

Figure 20: Averaging kernels of O_3 for bands A (left), B (middle) and C (right). A thick red line is an integration of the averaging kernel for each altitude, which indicates amount of information at that altitude. Averaging kernel altitudes and corresponding vertical resolutions are indicated on the right side of each plot.

In this calculation, we assume that the profiles correspond to the standard mid-latitude atmosphere (see Figure 21). The thick red line, which is an area of $\mathbf{a_i}$ (i^{th} row of $\mathbf{A}$) and is calculated by $\mathbf{a_i^T u}$ using a vector with unit elements $\mathbf{u}$, indicates the amount of information in the measurement (Rodgers, 2000). Bands A and B contain more information for the O_3 measurement than band C in the upper stratosphere because the center of the line in these two bands is located there. Band C contains more information in the low stratosphere than bands A or B, because the tail of the O_3 emission line is detected in band C. To retrieve the O_3 vertical profile at low stratosphere with high precision, band C plays a significant role (Section 17).

15 Error Analysis

Other possible error sources for O_3 retrieval using SMILES are:

- Pointing error,
- Bias error from the a priori profile,
- Uncertainty of the atmospheric temperature,
- Forward model parameter errors.

An error of pointing is one of the most significant issues for atmospheric remote sensing measurements using limb-viewing instruments. We retrieve the offset of the pointing to reduce the effect from the pointing error and the details of pointing retrieval for SMILES are described in Takahashi et al. (2009).

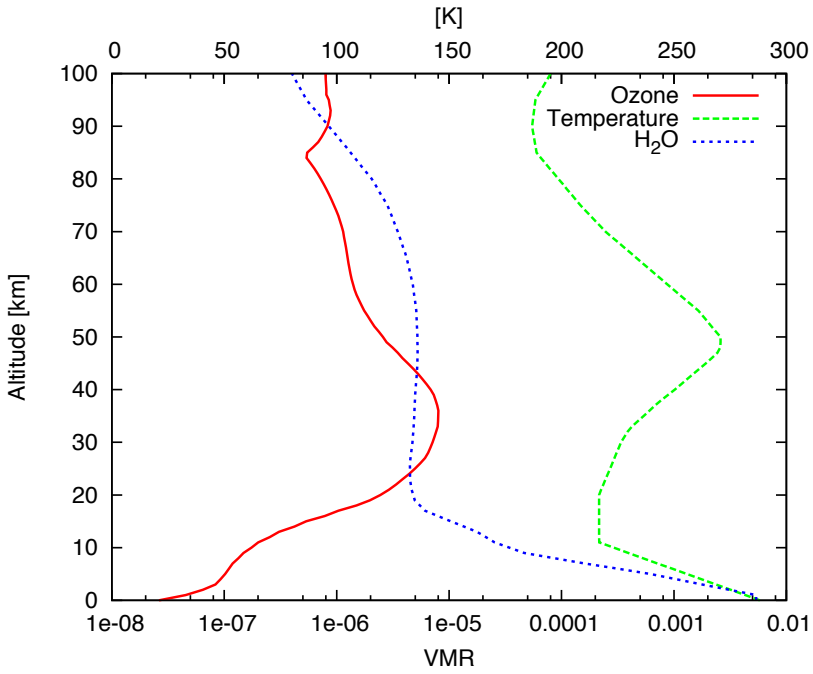

Figure 21: The standard mid-latitudes atmosphere profiles have been used in this study. The solid red line is the ozone profile, the dotted blue line is the atmospheric temperature profile and the dashed green line is H_2O profile.

The bias errors from the a priori assessment of the O_3 profiles are estimated in Figure 22. It shows additional errors caused by the differences between the true and the a priori O_3 profiles in the case of the mid-latitudes and the tropics. Here, the true profiles are the profiles that are used for the calculations of the simulated measurement vector ($\mathbf{y}$). Systematic errors are derived by comparing these true profiles with profiles retrieved by the software when a bias is applied to one of the input parameters (in this case the O_3 a priori profile). The additional error, $\sigma_{\delta x_i}$, is defined by

$$\sigma_{\delta x_i} = \sqrt{\sigma_i^2 + (\delta x_i)^2} - \sigma_i. \tag{27}$$

the σ_i is the square root of the i^{th} diagonal component of $\mathbf{S}$ and δx_i is i^{th} component of $\delta\mathbf{x}$ ($\delta\mathbf{x} = \mathbf{x_{true}} - \mathbf{x_{ret}}$), where $\mathbf{x_{true}}$ and $\mathbf{x_{ret}}$ are the true and the retrieved profiles, respectively. The error ratio is represented by $\sigma_{\delta x_i}/\mathbf{x_a}$. Excluding the case of the –50% difference (i.e. $\mathbf{x_{true}}$ is half of $\mathbf{x_a}$), the additional errors are less than 3% in the stratosphere for both mid-latitudes and the tropics. Since we prepared a priori profiles of O_3 for every 10–degree latitude grids, every month and day and night, the influence of the a priori profiles should be insignificant for the O_3 retrieval.

Next, we show effects from the uncertainty of the atmospheric temperature. The standard approach in the previous millimeter and submillimeter limb sounders (Waters et al., 1999; Read et al., 2006) is to derive the information on the atmospheric temperature from the oxygen emission lines (Livesey et al., 2006; Wehr et al., 1998). Since there is no oxygen line in the SMILES measurement bands, the atmospheric temperature can be derived from the O_3 emission line at 625.37 GHz (NASDA and CRL, 2002; Verdes et al., 2002; Baron et al., 2001). Figure 23 shows a comparison of the information con-

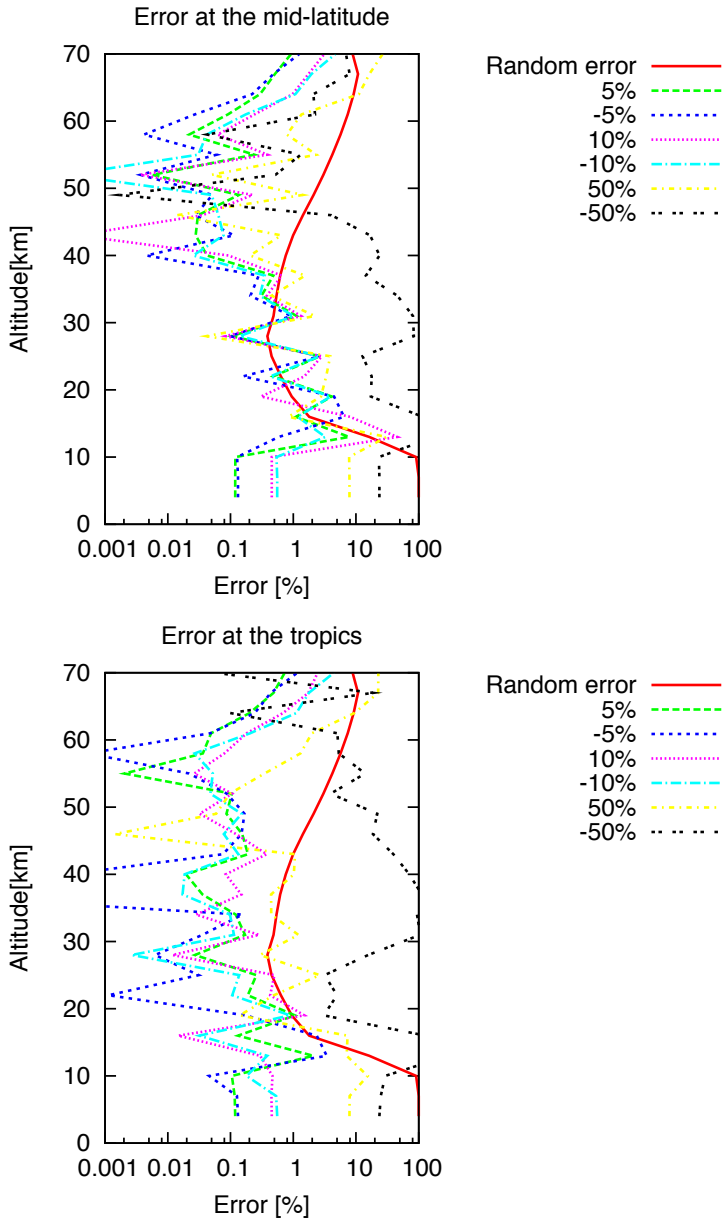

Figure 22: Estimations for the influence of priori profiles in O_3 retrieval (in this case, a priori profiles are same as initial profiles). The solid red line is the random error of O_3. The other lines are additional errors between the true profiles of O_3 and the retrieved profiles of O_3 that are the final results of the iteration process in the cases where the differences between the a priori profiles and true profiles are $\pm 5\%$, $\pm 10\%$, and $\pm 50\%$. (top: mid-latitudes, bottom: tropics).

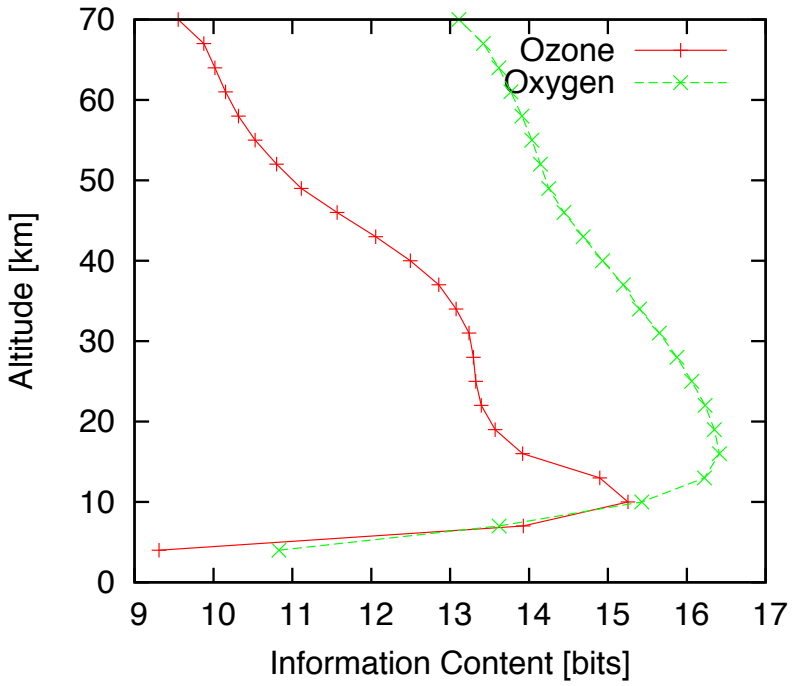

Figure 23: Information content of O_3 at 625.37 GHz (red/solid line) and oxygen at 118 GHz (green/dashed line).

tent (Rodgers, 1998) of the atmospheric temperature for the O_3 emission line at 625.37 GHz and for the oxygen emission line at 118 GHz under the same conditions as SMILES. It indicates that the atmospheric temperature can be retrieved by using the O_3 emission line, although it is not as precise as from the oxygen emission line especially in the upper stratosphere. The atmospheric temperature and O_3 vertical profiles are unknown quantities to be retrieved. Both of them can be retrieved from the same measurement because of the different frequency dependence of their weighting functions.

Figure 24 shows the effect of the atmospheric temperature uncertainty upon retrieved O_3 profiles. Each line is $\sigma_{\delta x_i}$ corresponding to the difference

between the true and the a priori profiles of atmospheric temperature, which are 1 K (red line), 2 K (green line), 5 K (blue line), and 10 K (pink line), respectively. If the difference between the true and a priori profiles is below 10 K, the additional error is below 1% in the stratosphere. Following this result, we will use the reanalysis and reprocessing data produced by Global Modeling and Assimilation Office (GMAO) of Goddard Space Flight Center (GSFC) for atmospheric temperature. By applying GMAO data, the error caused by the atmospheric temperature will be less than 1% in the stratosphere (Rienecker et al., 2007).

The forward model parameter errors in the launch-ready algorithm have been estimated in Takahashi et al. (2009). It shows that each forward model parameter error from optimizing the radiative transfer calculation and designing the accurate instrument functions (such as the instrumental field of view, the sideband rejection ratio of sideband separator, and the spectral responses of acousto-optic spectrometers) is below 0.01%. Errors associated with line parameters such as air-broadening parameters and partition functions were estimated by Verdes et al. (2005a). According to the paper, partition function errors do not introduce significant errors for most of the target species of SMILES except BrO. It is known that there are still some forward model parameter errors that have not been estimated such as spectroscopic parameters and cirrus clouds. To estimate and improve the accuracy of the retrieval, we have been estimating these errors using the real observation data.

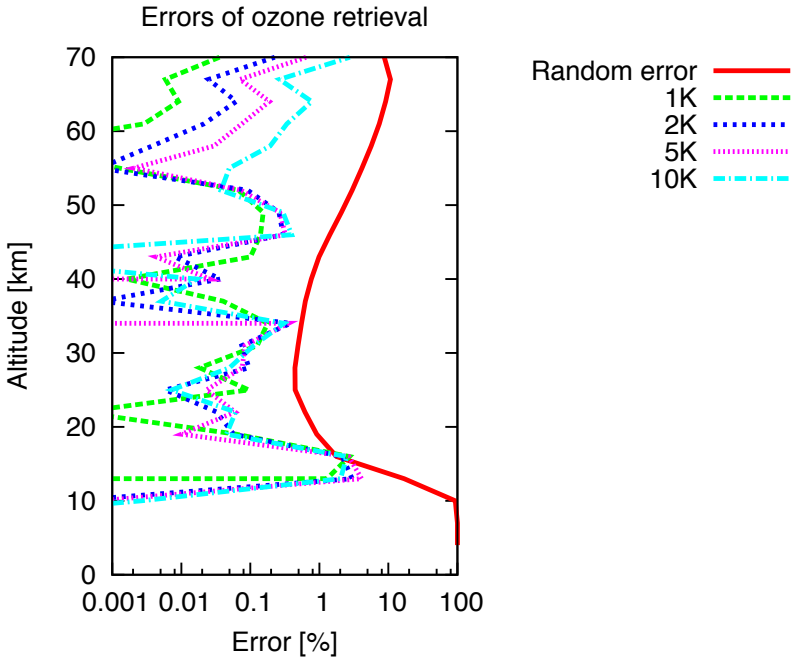

Figure 24: Estimation of the influence of uncertainty of initial and a priori profiles of atmospheric temperature (in this case, we retrieve atmospheric temperature and O_3 profile simultaneously and the priori profiles of atmospheric temperature are same as initial profiles). Lines are additional errors between the true profiles of O_3 and the retrieved profiles of O_3 that are the final results of the iteration process in the cases where the uncertainties of atmospheric temperature are 1 K (red/solid line), 2 K (green/dashed line), 5 K (blue/dotted line) and 10 K (pink/fine-dotted line).

16 Diurnal Variation of O_3 Abundance in the Upper Stratosphere

Ozone has a strong diurnal variation in the upper stratosphere and the mesosphere (Allen et al., 1984). Since the ISS is not in a sun-synchronous orbit and its orbital plane rotates every 60 days, SMILES can produce one day datasets that can describe the diurnal variation using 60 days SMILES observation data. In this section we estimate the capability of SMILES observations for the diurnal variation of ozone by investigations of the ozone random error at two extreme times, which are the midnight and the noon.

The solar occultation sensors (ACE, SAGEs, etc.) can measure in sunrise and sunset conditions. The scattering instruments can measure the diurnal variation only in the daytime but most of these instruments are on a sun-synchronous orbit, so their observations are limited within fixed local time. SMILES has an advantage in measuring diurnal variation but it has not been previously discussed (NASDA and CRL, 2002). Here, we study the retrieval capability of the diurnal variation with SMILES.

Figure 25 shows the random error from single-scan spectra of band A in the daytime (red/solid line) and in the nighttime (green/dashed line). Ozone a priori profiles in this estimation have been applied with the annually averaged and 10° degree zonal mean (35–44°N) (Froidevaux et al., 2008; Livesey et al., 2007) of the Aura/MLS version 2.2 data for day and night, respectively. At 70 km altitude ozone can be measured with 5% random error in the nighttime and, because of a low abundance, with 20% random error in the daytime.

SMILES is a powerful instrument to investigate O_3 chemistry in the upper

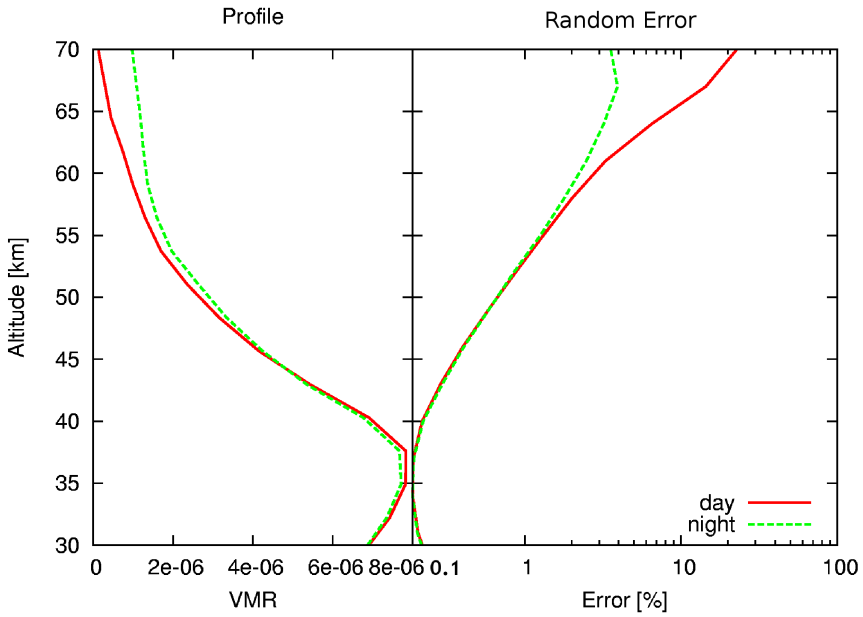

Figure 25: Diurnal variability of the O_3 measurements. The left side of the figure shows the ozone profiles and the right figure shows the random error in the daytime (red/solid line) and in the nighttime (green/dashed line), respectively.

stratosphere and the mesosphere. To improve the random error, we apply the averaging algorithm (Livesey et al., 2006) in the high-altitude region. After averaging ten spectra, the random error at 70 km altitude is improved to 5% in the daytime and is 1% in the nighttime.

17 Retrieval Capability in the Lower Stratosphere and Upper Troposphere

In our early estimation (NASDA and CRL, 2002), it was stated that SMILES can measure O_3 profiles above 20 km (i.e. SMILES cannot measure the lower stratosphere). The results of the early estimation were based on the retrieval using a single band independently. In this section we study the retrieval capability of ozone below 20 km using two bands combinations because SMILES mounts two Acousto-Optical Spectrometer and measures the two bands simultaneously. Also we estimate effects of cirrus clouds.

17.1 Two-Bands Simultaneous Retrieval

SMILES measures two bands simultaneously as mentioned in Section 13. We consider a possibility of improving the random error for O_3 by the simultaneous retrieval of two bands (Figure 26) in the cases of the mid-latitudes (top) and the tropics (bottom). Since SMILES has poor coverage in the polar region, we focus on the mid-latitudes and the tropics. We use the profiles of the standard 45°N and 0°N atmosphere for mid-latitude and the tropics estimation, respectively. The lines on the left of Figure 26 are the profiles of O_3 (red/solid line), temperature (green/dashed line), and H_2O (blue/dotted line).

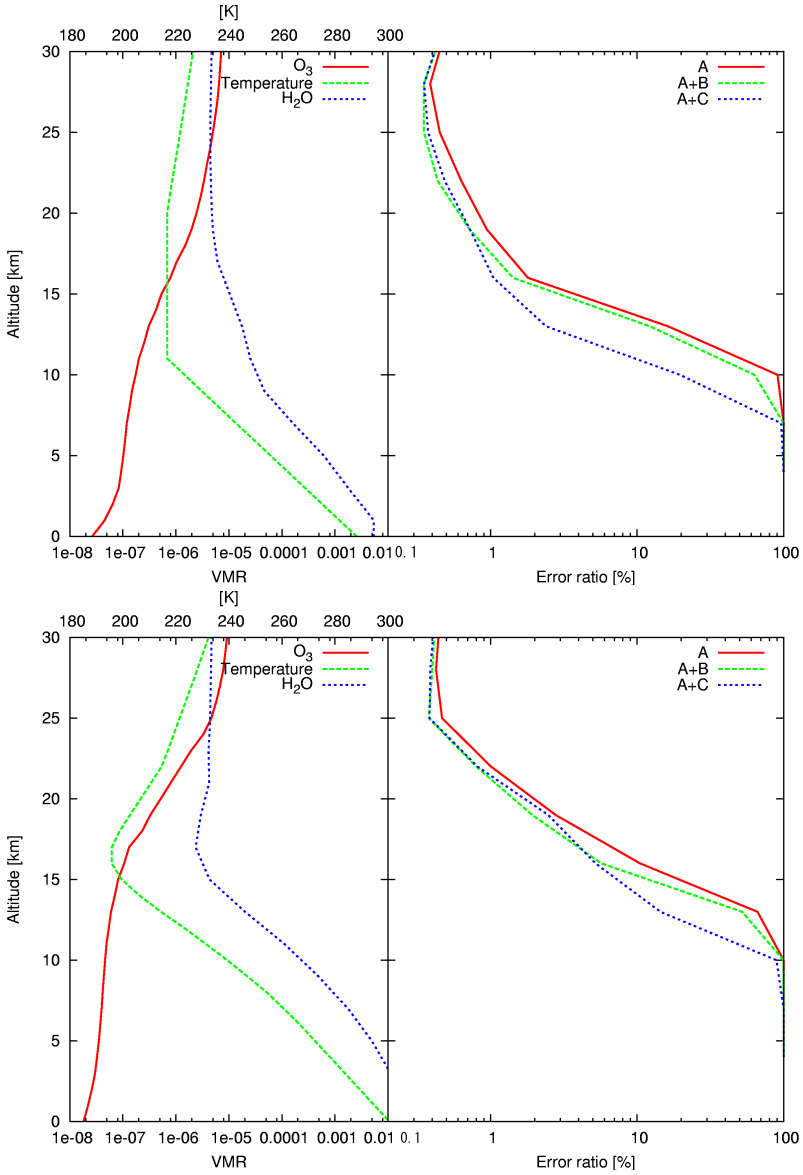

Figure 26: Results of synthetic retrievals using different bands. The left side of the figure shows the profiles used in each simulation and the right side of the figure shows the random error in the case of the mid-latitudes (top) and the tropics (bottom). The lines on the left side of the figure are the profiles of O_3 (red/solid line), temperature (green/dashed line), and H_2O (blue/dotted line). The lines on the right side of the figure are the random error of O_3 using band A only (red/solid line), using bands A and B (green/dashed line), and using bands A and C (blue/dotted line).

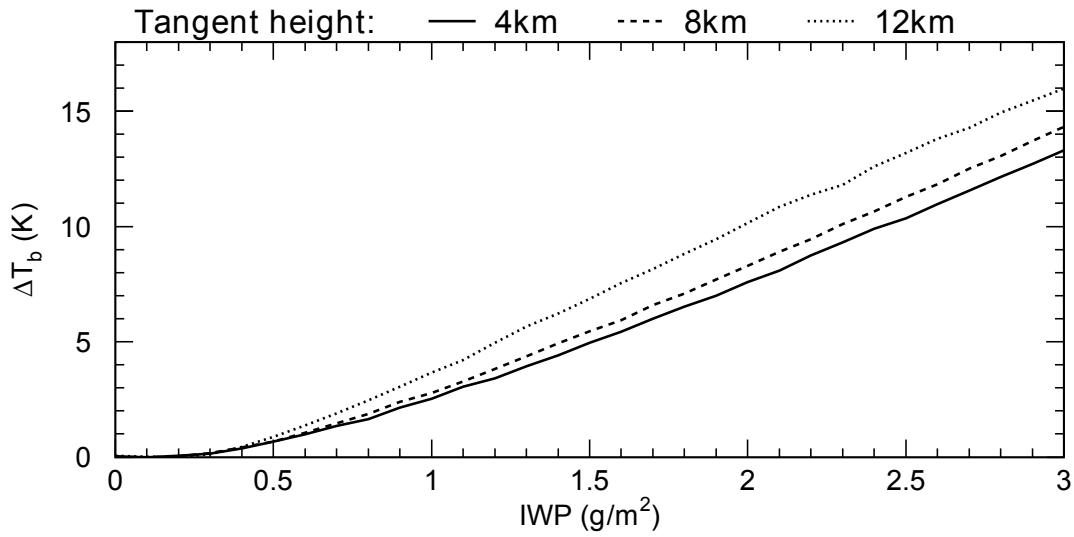

Figure 27: Relationship between the ice water path (IWP) and the brightness temperature depression due to cirrus clouds. The tangent altitudes are 4 km (solid line), 8 km (dashed line), and 12 km (dotted line) and the cloud layer is assumed to be uniformly between 12 km and 13 km.

The right side of Figure 26 shows the random errors of O_3 by using (1) band A only (red line), (2) both bands A and B (green line), and (3) both bands A and C (blue line). By using bands A and C simultaneously, the random error is less than 5% above 13 km in the mid-latitudes and above 15 km in the tropics. In contrast, the random error at 13 km in the mid-latitudes is approximately 50% using only band A. The random error at 15 km in the tropics is approximately 40% using only band A and 30% using both bands A and B. It indicates that the simultaneous retrieval of bands A and C improves the random error especially in the lower stratosphere under the clear sky conditions.

17.2 Effects from Cirrus Clouds

The O_3 profile cannot be retrieved if there are thick clouds such as cumulonimbi in the lines of sight of SMILES, but we have not yet discussed the possibility of the O_3 retrieval under the thin clouds like cirrus clouds existence. Here, we discuss the possibility of retrieval of the O_3 profile under the condition of cirrus clouds existence. It is important to estimate the cirrus clouds because they (including invisible thin clouds) exist globally with high possibility below the lower stratosphere.

Figure 27 shows the relationship between the ice water path (IWP) and the brightness temperature depression because of cirrus clouds estimated with the atmospheric radiative transfer simulator (Bühler et al., 2005). A uniform cloud layer between 12 and 13 km is assumed. The brightness temperature depressions are 1 K in the case of IWPs = 0.5 g/m^2 and 3 K in the case of IWPs = 1.0 g/m^2.

We estimate the error, $\delta\mathbf{x}$, due to the cirrus clouds whose IWPs are equal to 0.5 g/m^2 and 1.0 g/m^2 in the mid-latitudes and the tropics (See Figure 28). The error ratio in Figure 28 is defined $\delta\mathbf{x}/\mathbf{x_a}$. $\delta\mathbf{x}$ increases rapidly below 13 km in the case of IWPs = 0.5 g/m^2 and below 16 km in the case of IWPs = 1.0 g/m^2 in the mid-latitudes. It means that the O_3 profile in the mid-latitudes cannot be retrieved below 13 km (i.e. around the tropopause altitude) if there are clouds with IWP greater than 0.5 g/m^2 (uniformly distributed between 12 km and 13 km).

In the tropics, the clouds whose IWP is less than 1.0 g/m^2 have little effect on the O_3 retrieval. The retrieval errors increase less than approximately 10% above 16 km. SMILES has a capability to measure O_3 distributions above

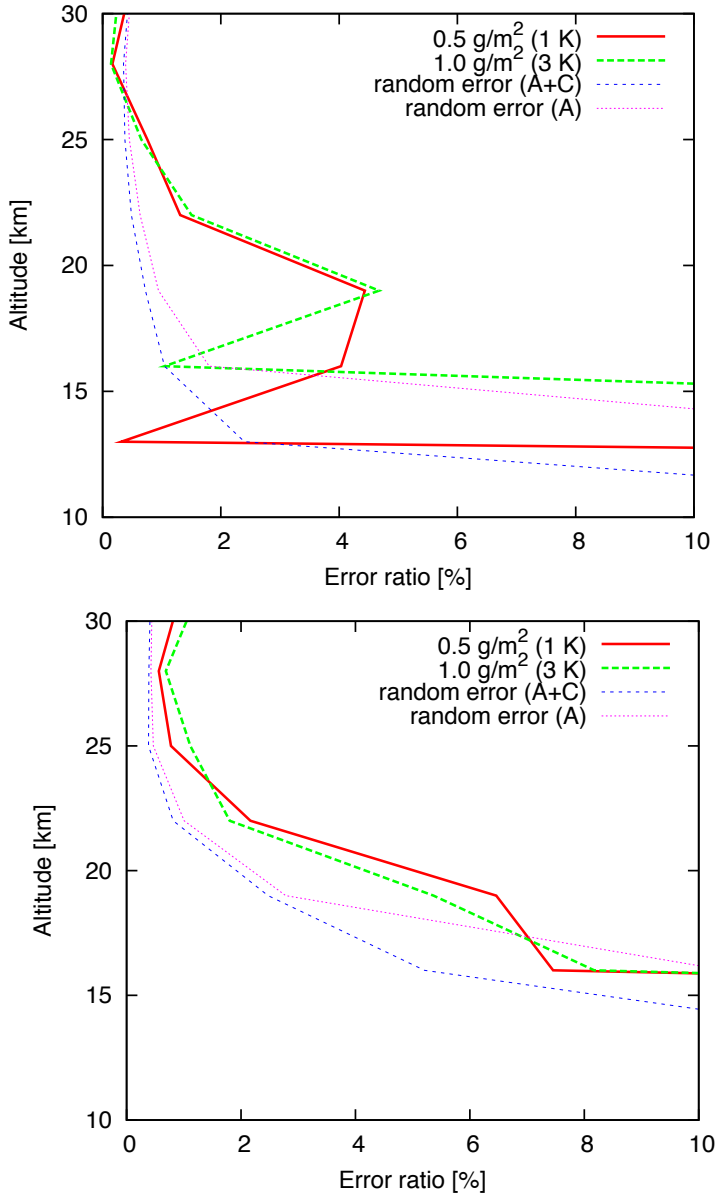

Figure 28: Effects from the cirrus clouds whose IWP are 1.0 (red/solid line) and 0.5 (green/dashed line) g/m^2 with the random error of the bands A and C (blue/dotted line) and A only (pink/fine-dotted line) in the case of the mid-latitudes (top) and the tropics (bottom).

16 km that can be retrieved with an error below 10% in the tropics, even in a presence of thin clouds between 12 and 13 km.

18 Conclusion

We have estimated O_3 random error with its altitude range by the SMILES observations. In the early estimations in NASDA and CRL (2002), it was estimated that the random error of O_3 vertical profiles was better than 5% from 20 to 45 km and 10% from 18 to 53 km but these errors includes the random error and some systematic errors together. In this study, we reveal and classify the random error and other systematic errors. Furthermore we estimated the retrieval capability of the diurnal variation and the lower stratosphere and upper troposphere for the first time in this study.

The best random error is found to be about 0.4% at 28 km and better than 5% between 15 and 70 km in the nighttime and between 15 and 55 km in the daytime. This high precision is mainly due to the low system-noise temperature of SMILES, which is less than 400 K. In rough estimation, the random error of SMILES is also one order of magnitude better than similar previous sensors. The systematic errors are estimated in section 15. We mentioned the systematic errors for the bias error of the a priori profile and uncertainty of the atmospheric temperature. The first one is almost same as the random error at 28 km (the minimum point of the random error), and the second one is 0.2% at 28km. Therefore, the total error, which is the sum of the random error and the systematic errors, at 28 km is approximately 1%.

Above 55 km O_3 profiles can be retrieved with the random error better

than 5% in the nighttime. In the daytime, the random error gets worse because the O_3 abundance in this altitude region decreases. Since the high-altitude region is important for investigations of the O_3 diurnal variation in the upper stratosphere, we will adopt the averaging algorithm of MLS (Livesey et al., 2006), which is unsusceptible to the bias of the a priori profile to improve the random error. After averaging ten spectra, the random error can be improved from 20% (single scan) to 5% (averaging ten times). We are planning to use the averaging scheme after sufficient validation of the single-scan retrieval.

Furthermore, using simultaneous retrievals of bands A and C, random errors above 15 km in the tropics and above 13 km in the mid-latitudes are expected to be about 5% under clear sky conditions. The SMILES observations are expected to provide information on O_3 vertical distribution from the lower to upper stratosphere. In previous studies the effect of clouds below 20 km has been found to be non-negligible, however, no quantitative tests were performed. Here, we have found that in a presence of thin clouds between 12 and 13 km (with IWP less than 1.0 g/m^2) O_3 can be retrieved only above 16 km for both mid-latitudes and tropics.

There are some important issues to resolve in the low-altitude region such as uncertainty of H_2O abundance and the continuum model. In the SMILES measurement bands, there is no H_2O line but there is the continuum component. In the launch-ready algorithm, the continuum components are fitted by the MPM-89 model (Liebe, 1989) and the components that can not be removed are fitted by a slope function. It works reasonably well but we continue to research strategies to improve data quality.

Finally, we mention some important issues to resolve, such as pointing error and spectroscopic parameters errors. In our algorithm, the offset of the pointing is retrieved (the details are in (Takahashi et al., 2009)) and this algorithm works properly in real data processing. For the spectroscopic parameters, detailed study is now performed with real data.

References

Allen M, Lunine JI, Yung YL, The vertical distribution of ozone in the mesosphere and lower thermosphere. J. Geophys. Res;1984;89;48414872.

Baron P, Merino F, Murtagh D, Simultaneous retrievals of temperature and volume mixing ratio constituents from non-oxygen Odin submillimeter bands. Opt;2001;40(33);61026110.

Bernath PF, McElroy CT, Abrams MC, Boone CD, Butler M, Camy-Peyret C, Carleer M, Clerbaux C, Coheur PF, Colin R, DeCola P, DeMazie M, Drummond JR, Dufour D, Evans WF, Fast H, Fussen D, Gilbert K, Jennings DE, Llewellyn EJ, Lowe RP, Mahieu E, McConnell JC, McHugh M, McLeod SD, Michaud R, Midwinter C, Nassar R, Nichitiu F, Nowlan C, Rinsland CP, Rochon YJ, Rowlands N, Semeniuk K, Simon P, Skelton R, Sloan JJ, Soucy MA, Strong K, Tremblay P, Turnbull D, Walker K, Walkty I, Wardle DA, Wehrle V, Zander R, Zou J Atmospheric Chemistry Experiment (ACE):Mission overview. Geophys. Res. Lett., 32, L15S01, doi:10.1029/2005GL022386.

Bovensman H, Burrows JP, Buchwitz M, Frerick J, Noël S, Rozanov VV, Chance KV and Goede APH, SCIAMACHY: Mission objectives and measurement modes. J. Atmos.Sci;1999;56(2);127-150

Bevilacqua RM, Hoppel K, Hornstein J, Lucke R, Shettle E, Ainsworth T, Debrestian D, Fromm M, Lumpe J, Krigman S, Glaccum W, Olivero J, Clancy RT, Rusch D, Randall C, Dalaudier F, Deniel C, Chassefiere E,

Brogniez C, Lenoble J, First results from POAM II: The Dissipation of the 1993 Antarctic Ozone Hole Geophys. Res. Lett.;1995;21;909-912.

Bühler SA, Eriksson P, Kuhn T, Engeln A, and Verdes C. ARTS, The atmospheric radiative transfer simulator. JQSRT;2005;91(1);65-93.

European Space Agency: Envisat, MIPAS An instrument for atmospheric chemistry and climate research, ESA Publications Division, ESTEC, P.O.Box 299,2200 AG NOOrdwijk, The Netherlands, SP-1229

Fischer H and Oelhaf H, Remote sensing of vertical profiles of atmospheric trace constituents with MIPAS limb-emission spectrometers. Appl. Opt;1996;35(16);2787796

Froidevaux L, Jiang YB, Lambert A, Livesey NJ, Read WG, Waters JW, Browell EV, Hair JW, Avery MA, McGee TJ, Twigg LW, Sumnicht GK, Jucks KW, Margitan JJ, Sen B, Stachnik RA, Toon GC, Bernath PF, Boone CD, Walker KA, Filipiak MJ, Harwood RS, Fuller RA, Manney GL, Schwartz MJ, Daffer WH, Drouin BJ, Cofield RE, Cuddy DT, Jarnot RF, Knosp BW, Perun VS, Snyder WV, Stek PC, Thurstans RP, Wagner PA, Validation of Aura Microwave Limb Sounder stratospheric ozone measurements. JGR;2008;113;D15S20, doi:10.1029/2007JD008771.

Harris N, Hudson R, and Phillips C, Assessment of Trends in the Vertical Distribution of Ozone. SPARC Rep;1;289;World Meteorol. Org.;Geneva;Switzerland;1998

Kikuchi K,Nishibori T,Ochiai S,Ozeki H, Irimajiri Y,Kasai Y, Koike M,Manabe T, Mizukoshi K, Murayama Y,Nagahama T,Sano T,

Sato Ryota,Seta M,Takahashi C. Takayanagi M, Masuko H,Inatani J,Suzuki M, and Shiotani M, Overview and Early Results of the Superconducting Submillimeter-Wave Limb-Emission Sounder (SMILES). JGR;2010;15;D23306;12.

Levenberg K, A method for the solution of certain problems in least squares Quart.Appl.Math;1944;2;164-168.

Liebe HJ, MPM-an atmospheric millimeter-wave propagation model. Int J Inf Millim Waves;1989;10(6):631-50.

Livesey NJ, Snyder WV, Read WG, Wagner PA, Retrieval algorithms for the EOS Microwave limb sounder (MLS). IEEE-MTT, 44(5), 1144–1155, 2006. doi 10.1109/TGRS.2006.872327

Livesey NJ,Read GW, Lambert A, Cofield ER, Cuddy TD, Froidevaux L, Fuller AR, Jarnot FR, Jiang HJ, Jiang BY, Knosp WB, Kovalenko JL, Pickett MH, Pumphrey CH, Santee LM, Schwartz MJ, Stek CP, Wagner PA, Waters WJ, and Wu LD, Version 2.2 Level 2 data quality and description document JPL D-33509;May 22,2007.

Marquardt DW, An algorithm for the least-squares estimation of nonlinear parameters SIAM J.Appl.Math;1963;11;431-441.

Murtagh D, Frisk U, Merino F, Ridal M, Jonsson A, Stegman J, et al., An overview of the previous termOdinnext term atmospheric mission. Can J Phys;2002;80;30919.

NASDA/CRL, JEM/SMILES mission plan, Version 2.1.[Online]. Available: http://smiles.tksc.nasda.go.jp/document/indexe.html; 2002

Ochiai S, Kikuchi K, Nishibori T, Manabe T, Ozeki H, Mizukoshi K, Ohtsubo F, Tsubosaka K, Irimajiri Y, Sato R, and Shiotani M, Performance of JEM/SMILES in orbit. 21th Int'l Symp. Space Terahertz Technol., S8.1, (Oxford, UK), March 2010.

Pickett HM, Poynter RL, Cohen EA, Submillimeter, millimeter, and microwave spectral line catalogue. Technical Report JPL Publication 80-23,Rev.3,JPL, 1992.

Read WG, Shippony Z, Schwartz MJ, Livesey NJ, and Snyder WV, The Clear-sky Unpolarized Forward Model for the EOS Aura Microwave Limb Sounder (MLS). IEEE Trans. Geosci. and remote sens;2006;44(5).

Rienecker MM, Suarez MJ, Todling R, Bacmeister J, Takacs L, Liu HC, Gu W, Sienkiewicz M, Koster RD, Gelaro R, Stajner I, and Nielsen JE, The GEOS–5 data assimilation system:Documentation of versions 5.0.1, 5.1.0, and 5.2.0, Tech. Rep. Ser. on Global Modeling and Data Assimilation. NASA/TM;2007;104;606;27

Rodgers CD, Retrieval of atmospheric temperature and composition from remote measurements of thermal radiation. Rev Geophys and Space Phys;1976;14(4);609-624.

Rodgers CD, Characterization and error analysis of profiles retrieved from remote sounding measurements. JGR;1990;95(5);5587-5595.

Rodgers CD, Information content and optimisation of hight spectral resolution remote measurement. ASR;1998;21;361–367.

Rodgers CD, Inverse methods for atmospheric sounding: theory and practice, Series on atmospheric, oceanic and planetary physics, vol.2. Singapole, World Scentific; 2000

Rusch DW, Bevilacqua RM, Randall CE, Lumpe JD, Hoppel KW, Fromm MD, Debrestian DJ, Olivero JJ, Hornstein JS, Guo F, Shettle EP, Validation of POAM II Ozone Measurements with Coincident MLS, HALOE, and SAGE II Observations. JGR;1997;102(23);615–627

Russell JM, Gordley LL, Park JH, Drayson SR, Hesketh DH, Cicerone RJ, Tuck AF, Frederick JE, Harries JE, and Crutzen P, The Halogen Occultation Experiment. JGR; 1993;98;D6;10;777–797.

Takahashi C, Ochiai S, Suzuki M, Operational Retrieval Algorithms for JEM/SMILES Level2 Data Processing System, JQSRT; 2009; doi:10.1016/j.jqsrt.2009.06.005

Verdes C, Bühler SA, Engeln A, Kuhn T, Kuenzi K, Eriksson P, and Sinnhuber BM, Pointing and Temperature Retrieval from Millimeter/Sub-Millimeter Limb Soundings. JGR; 2002; 107(D16); 4299;doi:10.1029/2001JD000777.

Verdes C, Bühler SA, Perrinb A, Flaudb JM, Demaisonc J, Wlodarczakc G, Colmontc JM, Cazzolid G, and Puzzarinid C, A sensitivity study on spectroscopic parameter accuracies for a mm/sub-mm limb sounder instrument. J. Mol. Spectrosc;2005a;229(2);266-75.

Verdes C, Engeln A, and Bühler SA, Partition function data and impact on

retrieval quality for a mm/sub-mm limb sounder. JQSRT;2005b;90(2);217-38.

Waters JW, Read WG,Froidevaux L, Jarnot RF, Cofield RE, Flower DA, Lau GK, Pickett HM, Santee ML, Wu DL, Boyles MA, Burke J. R, Lay R. R, Loo M. S, Livesey N. J, Lungu TA, Manney GL, Nakamura LL, Perun VS, Ridenoure BP, Shippony Z, Siegel PH, Thurstans RP, Harwood RS, Pumphrey HC, and Filipiak MJ. The UARS and EOS Microwave Limb Sounder (MLS) experiments. J.Atmos.Sci.;1999;56;194-218.

Wehr T, Bühler SA, Englen A, Kunzi K, and Langen J, Retrieval of Spectroscopic Temperatures from Space Borne Mcrowave Limb Sounding Measurements, J Geophys. Res., 103, 25997-26006, 1998.

WMO (World Meteorological Organization): Scientific assessment of ozone depletion: 2006, WMO Global Ozone Res. and Monit. Project, Rep. 50, World Meteorol. Org., Geneva, 2007.

Wu DL, Austin RT, Deng M, Durden SL, Heymsfield AJ, Jiang JH, Lambert A, Li JL, Livesey NJ, McFarquhar GM, Pittman JV, Stephens GL, Tanelli S, Vane DG, and Waliser DE, Comparisons of global cloud ice from MLS, CloudSat, and correlative data sets. JGR;2009;114;doi:10.1029/2008JD009946

Overall Summary

The purpose of this work is to develop the launch ready retrieval algorithm with the highly accurate forward model and to clarify the capability of ozone measurement by SMILES.

SMILES have been launched on 11 September 2009 by H-II Transportation Vehicle (HTV) and have begun atmospheric observations on 12 October. The SMILES had achieved the system temperature was less than 400 K. The system temperature was realized better than specific value of 700 K. The measured data by SMILES were retrieved and profiles of the target species were produced as soon as the data had downloaded in the ground data processing system without problems. The measured SMILES data have been able to be retrieved by using the launch ready retrieval algorithm shown in Chapter II without any significant problems. The processing speed achieved as we expected. Appendix shows the results of ozone retrieval by the measured data using this algorithm. It shows that the SMILES data are consistent with the MLS data. For the other standard products, the retrieval processing was almost successful. It provided one of the evidence for the effectiveness of this retrieval algorithm. Furthermore, it was confirmed that the ability of processing was also sufficient.

In Chapter III, O_3 random error with its altitude range by the SMILES observations and systematic errors are estimated. The retrieval capability of the diurnal variation and the lower stratosphere and upper troposphere are

also estimated for the first time in this study. It provide that the best random error is found to be about 0.4% at 28 km and better than 5% between 15 and 70 km in the nighttime and between 15 and 55 km in the daytime.These error is roughly one order of magnitude better than similar previous sensors. The total error, which is the sum of the random error and the systematic errors, at 28 km is approximately 1% . In the case of the upper stratosphere in the daytime, the random error can be improved from 20% (single scan) to 5% (averaging ten times) by averaging ten spectra. Meanwhile, in the lower stratosphere using simultaneous retrievals of bands A and C, random errors above 15 km in the tropics and above 13 km in the mid-latitudes are expected to be about 5% under clear sky conditions. Here, we have found that in a presence of thin clouds between 12 and 13 km (with IWP less than 1.0 g/m^2) O_3 can be retrieved only above 16 km for both mid-latitudes and tropics. The SMILES observations are expected to provide information on O_3 vertical distribution from the lower to upper stratosphere.

SMILES stopped the observation because of the hardware problem in April 2010 unfortunately and it was working about half a year. The study for the retrieval algorithm is still continued and it is improved by using received data of half a year. There are some important issues to resolve using real data to improve data quality. For example, the uncertainty of H_2O is one of the big issue. In the launch-ready algorithm, the continuum components are fitted by the MPM-89 model (Liebe, 1989). It works reasonably well but we continue to research strategies. Others are pointing error and spectroscopic parameters errors. In our algorithm, the offset of the pointing is retrieved

and this algorithm works properly in real data processing. Some of the spectroscopic parameters in the launch-ready algorithm are used measured values in laboratories, but not all of them. It should be estimated with real data whether the spectroscopic parameters should be measured.

Acknowledgments

I would like to express my deep gratitude to Professor Masato Shiotani of the Research Institute for Sustainable Humanosphere (RISH), Kyoto University, for his enormous supports and insightful comments of this study. I am deeply grateful to Dr. Makoto Suzuki of the Institute of Space and Astronautical Science / JAPAN Aerospace Exploration Agency (ISAS/JAXA), whose opinions and information have helped me very much throughout the production of this study.

Special thanks to Professor Akira Mizuno and Associate Professor Tomoo Nagahama of the Solar-Terrestrial Environment Laboratory (STEL), Nagoya University, who gave me invaluable comments and suggestions to complete this thesis.

I would like to express my appreciation Dr. Masahiro Takayanagi, Mr. Takuki Sano, Dr. Koji Imai , Dr. Naohiro Manago of ISAS/JAXA and Dr. Chihiro Mitsuda and Mr. Hirotomo Taniguchi of Fujitsu FIP corporation, and Associate Professor Hiroo Hayashi of RISH, Kyoto University, who are the SMILES team members in ISAS/JAXA and study for the SMILES level 2 data processing and its algorithm together. They gave me valuable cooperations to my study and invaluable discussion that make my research of great achievement.

I also would like to thank the SMILES instrument team, Dr. Satoshi

Ochiai and Dr. Ken-ichi Kikuchi of National Institute of Information and Communications Technology (NICT), Dr. Toshiyuki Nishibori of JAXA, Professor Hiroyuki Ozeki of Toho University, Professor Takeshi Manabe of Osaka Prefecture University and Professor Shinji Inatani of National Astronomical Obsevatory of JAPAN, for their useful discussions and suggestions about the instrument characteristics. Finally, I am grateful to my family for their support and encouragement.

Appendix: Ozone retrieval by the measured data

SMILES have been launched on 11 September 2009 by H-II Transportation Vehicle (HTV) and it have begun atmospheric observations on 12 October 2009. SMILES have quit the atmospheric observation on 21 April 2010 because of the problem of the sub-millimeter local oscillator. SMILES have measured and stored about half years data of atmospheric observations, whose system noise temperature is better than 400 K (it better than the specification value of 700 K). In this appendix, some recent results for the ozone retrieval by using the SMILES measured data are shown.

The single scan spectra of the measured brightness temperature for band A, B, and C are shown in Figure 29 (Kikuchi et al., 2010). Since the system noise temperature is lower than specification value, weak emission lines like BrO and HO_2 can be seen in the single scan. Next, a sample of residual errors of the measured brightness temperature are shown in Figure 30 to verify the the retrieval algorithm. The residual errors of the measured brightness temperature is useful to check the validity of the retrieval processing. The residual errors in Figure 30 are almost less than 1 K for all tangent altitudes. The results show the good agreements between the measurement and the retrieval processing in most regions except line center. The retrieval processing is working as we expected but there are still remained the errors in the line shapes.

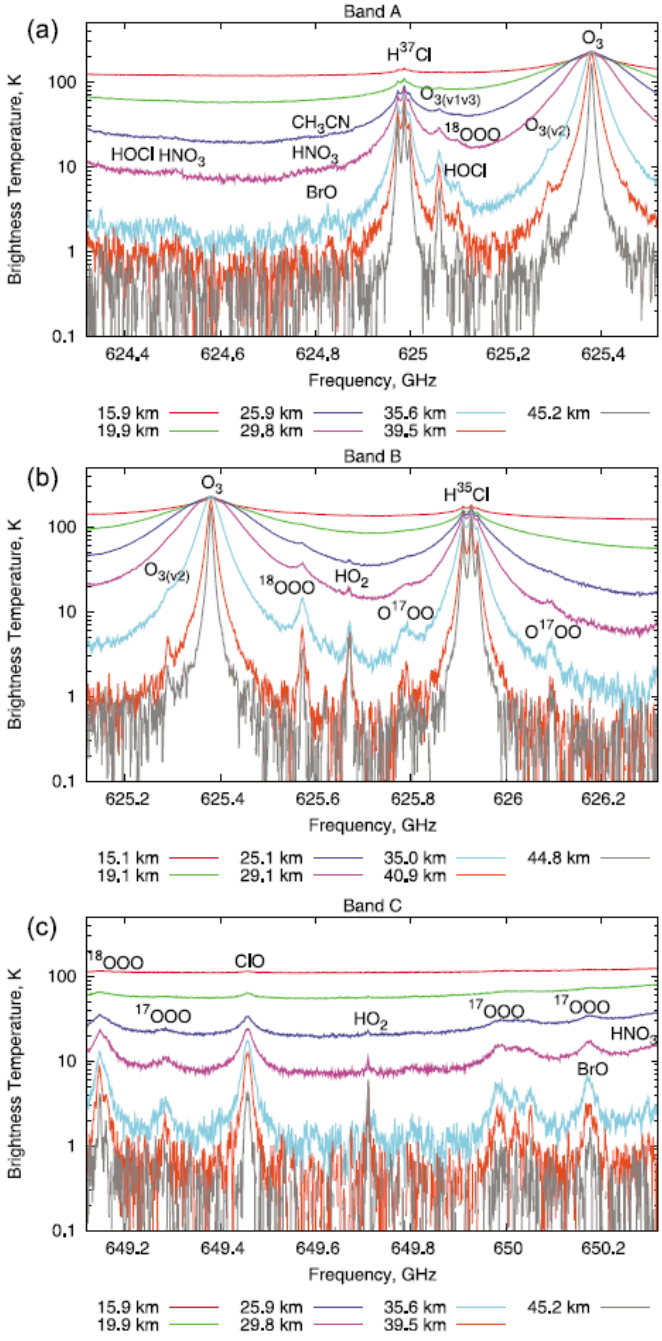

Figure 29: The measured spectra on 12 October 2009 at several tangent altitudes with log scale (Kikuchi et al., 2010). (a) is Band A, (b) is Band B, and (c) is Band C.

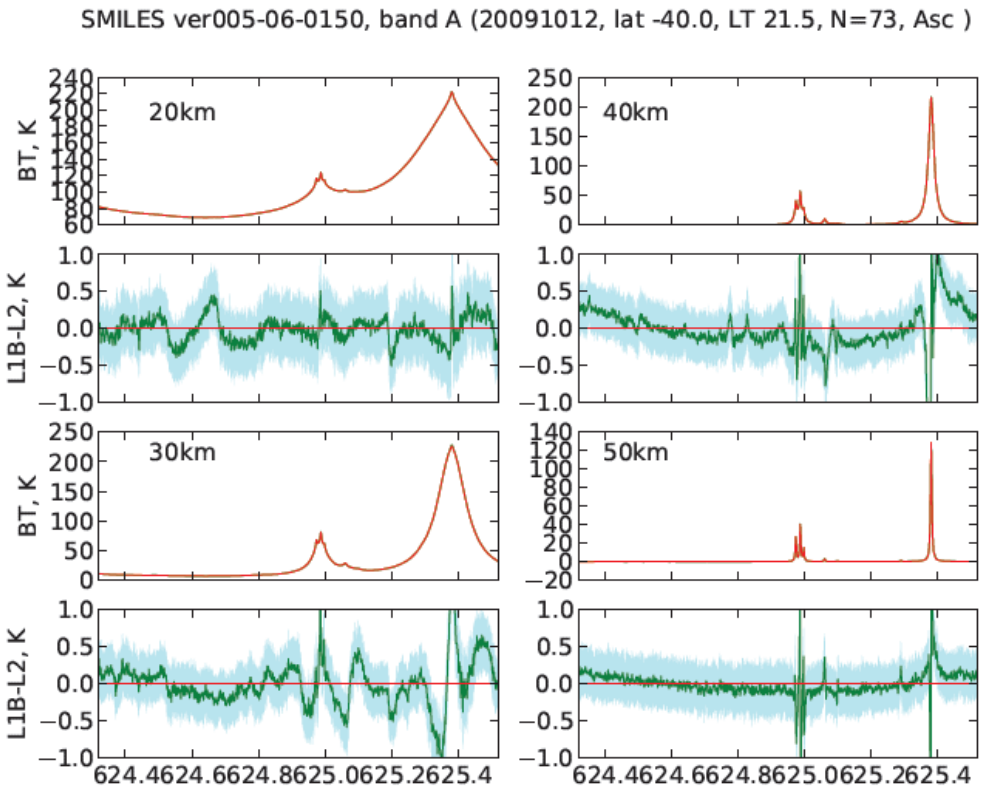

Figure 30: Brightness temperature and residual errors of the measured brightness temperature measured on 12 October 2009 at 20 km, 30 km, 40 km and 50 km altitudes.

The capability for the measurements of ozone diurnal variation by SMILES was discussed in Chapter III. Ozone mixing ratios processed by SMILES measured data are plotted with local times (see Figure 31). Figure 31 is ozone mixing ratio at 61 km altitude whose altitude must be appeared the diurnal variation (Garcia and Solomon, 1985). Ozone mixing ratios are decreasing in daytime and the ozone diurnal variations are clearly appeared in the SMILES measured data.

The first study for comparisons between SMILES and other sensors like MLS will be shown discussed in Kikuchi et al. (2010). Figure 32 (Kikuchi et al., 2010) shows the latitude-height sections of the zonal mean ozone on 12 October 2009 of SMILES (left) and AURA/MLS (right). This figure shows a good agreement with SMILES and MLS in the global scale dimensions. The comparison of the profiles of ozone concentration are in Figure 33 (Suzuki et al., 2010). It shows statistics estimation of comparison between SMILES and AURA/MLS for ozone retrieval profile using 284 coincidence data at the 55° N - 65° N latitude region. The difference between SMILES and AURA/MLS are less than 5% from 20 km to 45 km.

Finally, the status of the other target species is mentioned. Almost other target species are retrieved successful soon after receiving the measured data as same as ozone. Figure 33 (Suzuki et al., 2010) shows Statistics estimation of comparison between SMILES and AURA/MLS for HCl retrieval profile using coincidence data in the 55° N - 65° N latitude region. The difference between SMILES and AURA/MLS are less than 10% from 20 km to 45

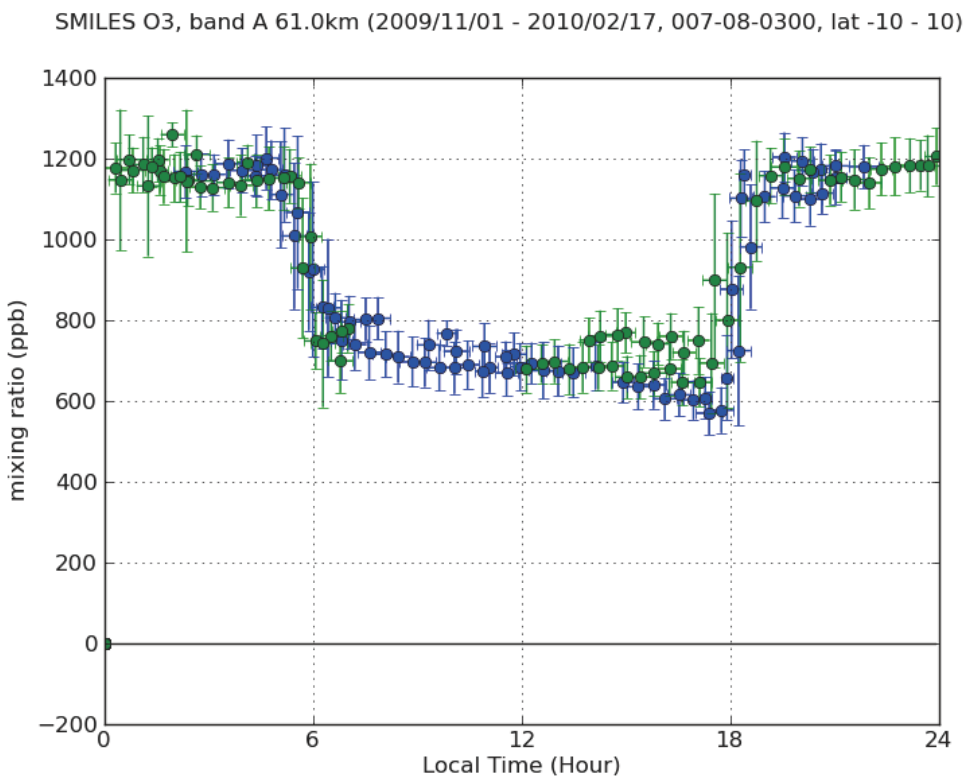

Figure 31: the measurements of ozone diurnal variation by SMILES. Green and blue points with error bars show ozone mixing ratios (ppb) at 61 km altitude of ascending and descending, respectively.

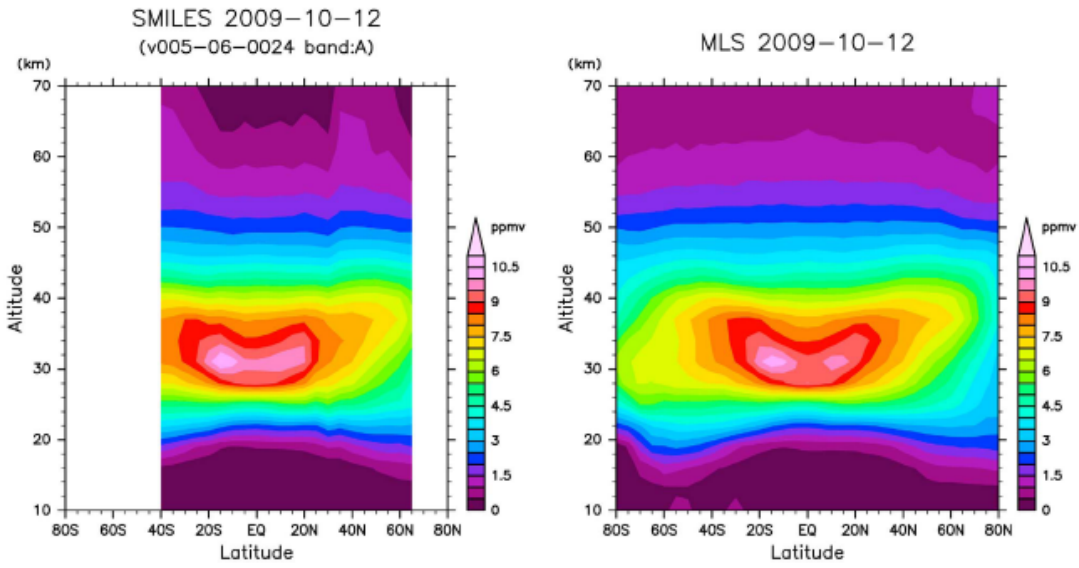

Figure 32: Latitude-height sections of the zonal mean ozone on 12 October 2009. Left side is SMILES and right side is AURA/MLS. In this case, data for daytime and nighttime are averaged (Kikuchi et al., 2010) .

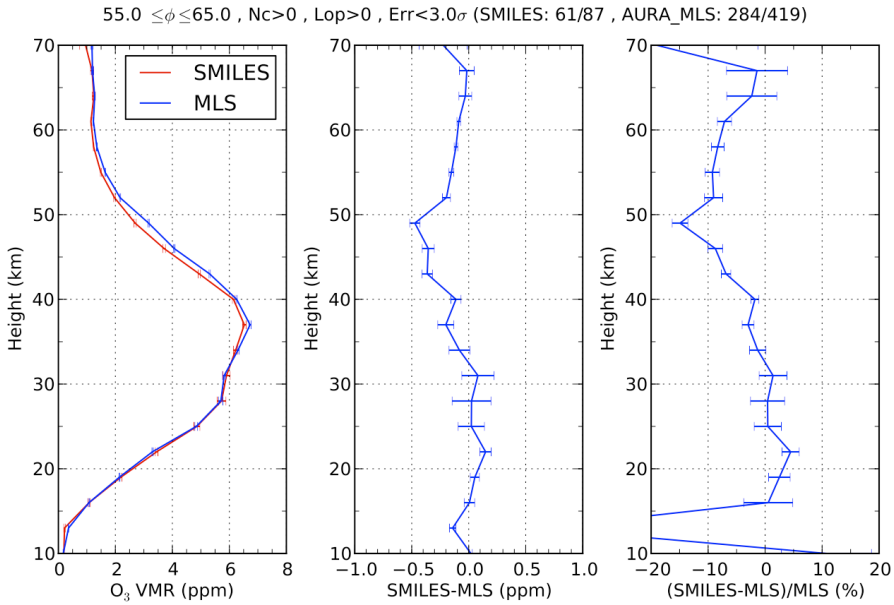

Figure 33: Statistics estimation of comparison SMILES and AURA/MLS for ozone retrieval profile, using coincident SMILES and AURA/MLS ozone profiles at the 55° N - 65° N latitude. Left: the mean profiles for SMILES (blue) and AURA/MLS (red), Middle: the differences between the SMILES and AURA/MLS profiles in mixing ratio, Right: the differences in percentage (Suzuki et al., 2010).

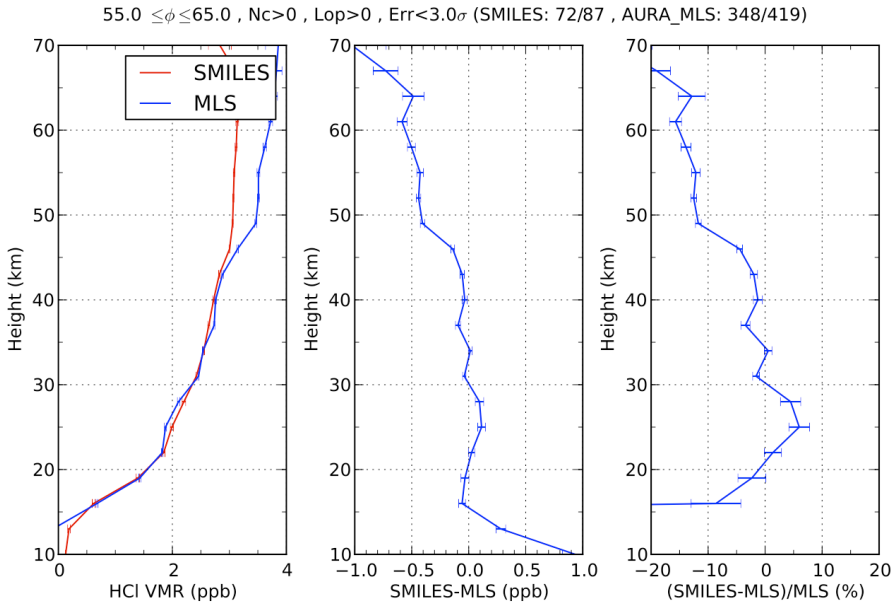

Figure 34: Statistics estimation of comparison SMILES and AURA/MLS for HCl retrieval profile using coincident SMILES and AURA/MLS ozone profiles in the 55° N - 65° N latitude region. Left: the mean profiles for SMILES (blue) and AURA/MLS (red), Middle: the differences between the SMILES and AURA/MLS profiles in mixing ratio, Right: the differences in percentage (Suzuki et al., 2010).

km. The recent papers of Shiotani et al. (2011) and Suzuki et al. (2010) shows the results of many more target species such as HNO_3 (see Figure 35). Some species especially whose spectra are mixable with baseline are difficult to retrieve. Further estimation for the baseline components such as water vapor needed for these species.

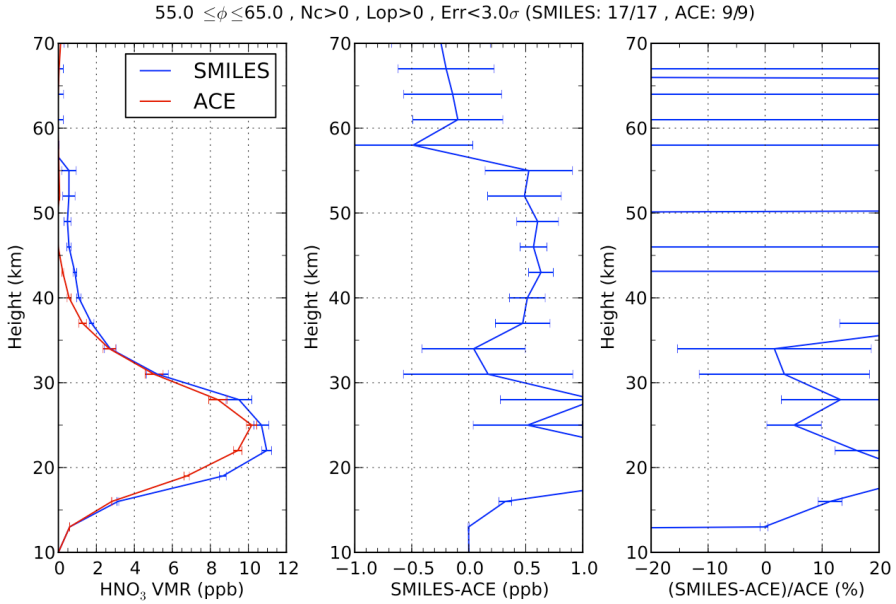

Figure 35: Example of HNO_3 coincidence compared with ENVISAT/MIPAS (MIPAS-IMK ver.40) at 67.1° N, 101.5° on Oct. 12, 2009. Two SMILES profiles (blue) are compared with 1 MIPAS profiles (red) (Suzuki et al., 2010).

References

Garcia, R and Solomon, S, The effect of breaking gravity waves. JGR;1985;90, 3850-3852.

Kikuchi K, Nishibori T,Ochiai S,Ozeki H, Irimajiri Y,Kasai Y, Koike M,Manabe T, Mizukoshi K, Murayama Y,Nagahama T,Sano T, Sato Ryota,Seta M,Takahashi C. Takayanagi M, Masuko H,Inatani J,Suzuki M, and Shiotani M, Overview and Early Results of the Superconducting Submillimeter-Wave Limb-Emission Sounder (SMILES). JGR;2010;15;D23306;12.

Shiotani M, Takayanagi M, Suzuki M, Sano T, SMILES Mission Team, Recent results from the Superconducting submillimeter-wave limb-emission sounder (SMILES) onboard ISS/JEM, SPIE;2011

Suzuki M, Mitsuda C, Takahashi C, Iwata T, Manago N, Sano T, Kikuchi K, Ochiai S, Imai K, Nishimoto E, Naito Y, Hayashi H, and Shiotani M, EARLY RESULTS FROM 4K-COOLED SUPERCONDUCTING SUBMM WAVE LIMB EMISSION SOUNDER SMILES ONBOARD ISS/JEM, International Archives of the Photogrammetry, Remote Sensing and Spatial Information Science, Volume XXXVIII, Part 8, Kyoto Japan 2010